

Robust Cooperative Manipulation without Force/Torque Measurements: Control Design and Experiments

Christos K. Verginis, *Member, IEEE*, Matteo Mastellaro, and Dimos V. Dimarogonas, *Member, IEEE*

Abstract—This paper presents two novel control methodologies for the cooperative manipulation of an object by N robotic agents. Firstly, we design an adaptive control protocol which employs quaternion feedback for the object orientation to avoid potential representation singularities. Secondly, we propose a control protocol that guarantees predefined transient and steady-state performance for the object trajectory. Both methodologies are decentralized, since the agents calculate their own signals without communicating with each other, as well as robust to external disturbances and model uncertainties. Moreover, we consider that the grasping points are rigid, and avoid the need for force/torque measurements. Load distribution is also included via a grasp matrix pseudo-inverse to account for potential differences in the agents' power capabilities. Finally, simulation and experimental results with two robotic arms verify the theoretical findings.

Index Terms—cooperative manipulation, multi-agent systems, adaptive control, robust control, unit quaternions, prescribed performance control.

I. INTRODUCTION

MULTI-agent systems have gained significant attention the last years due to the numerous advantages they yield with respect to single-agent setups. In the case of robotic manipulation, heavy payloads and challenging maneuvers necessitate the employment of multiple robotic agents. Although collaborative manipulation of a single object, both in terms of transportation (regulation) and trajectory tracking, has been considered in the research community the last decades, there still exist several challenges that need to be taken account by on-going research, both in control design as well as experimental evaluation.

Early works develop control architectures where the robotic agents communicate and share information with each other, and completely decentralized schemes, where each agent uses only local information or observers, avoiding potential communication delays (see, indicatively, [1]–[10]). Impedance and hybrid force/position control is the most common methodology used in the related literature [8]–[24], where a desired

impedance behavior is imposed potentially with force regulation. Most of the aforementioned works employ force/torque sensors to acquire feedback of the object-robots contact forces/torques, which however may result to performance decline due to sensor noise or mounting difficulties. When the grasping object-agents contacts are rigid, the need for such sensors is redundant, since the overall system can be seen as a closed-chain robot. Regarding grasp rigidity, recent technological advances allow end-effectors to grasp *rigidly* certain objects (e.g., [25] or electromagnetic technology), motivating the specific analysis.

Another important characteristic is the representation of the agent and object orientation. The most commonly used tools for orientation representation consist of rotation matrices, Euler angles, and the angle/axis convention. Rotation matrices, however, are not used very often in robotic manipulation tasks due to the difficulty of extracting an error vector from them. Moreover, the mapping from Euler angle/axis values to angular velocities exhibits singularities at certain points, rendering thus these representations incompetent. On the other hand, the representation using unit quaternions, which is employed in this work, constitutes a singularity-free orientation representation.

In addition, many works in the related literature consider known dynamic parameters regarding the object and the robotic agents. However, the accurate knowledge of such parameters, such as masses or moments of inertia, can be a challenging issue, especially for complex robotic manipulators.

Force/torque sensor-free methodologies have been developed in [4], [6], [8], [16], [19], [21], [22], [26], [27]; [16] develops a leader-follower communication-based scheme by partly accounting for dynamic parametric uncertainty, whereas [8] and [4] employ partial and full model information, respectively; [6] develops an adaptive control scheme that achieves boundedness of the errors based on known disturbance bounds, and [26] proposes an adaptive estimator for kinematic uncertainties, whose convergence affects the asymptotic stability of the overall scheme. In [21] and [22] adaptive fuzzy estimators for structural and parametric uncertainty are introduced, with the latter not taking into account the object dynamics; [27] develops an adaptive protocol that guarantees boundedness of the internal forces, and [19] employs an approximate force estimator for a human-robot cooperative task.

Unit quaternions in the control design of cooperative manipulation tasks have been employed in [11], where the authors address the gravity-compensated pose regulation of the grasped object, as well as in [12], where a model-based

The authors are with the Centre for Autonomous Systems and ACCESS Linnaeus Centre, KTH Royal Institute of Technology, Stockholm 10044, Sweden. Emails: {cverginis, matteoma, dimos}@kth.se.

This work was supported by the H2020 ERC Starting Grant BUCOPHSYS, the Swedish Research Council (VR), the Knut och Alice Wallenberg Foundation (KAW), the European Union's Horizon 2020 Research and Innovation Programme under the Grant Agreement No. 644128 (AEROWORKS), the Swedish Foundation for Strategic Research (SSF), and the EU H2020 Research and Innovation Programme under GA No. 731869 (Co4Robots).

force-feedback scheme is developed.

Full model information is employed in the works [1], [7], [9], [10], [13], [15], [17], [23]; [7] employs a velocity estimator, [23] uses a linearized model, and [14], [15] considers kinematic and grasping uncertainties. Adaptive control schemes are developed in [20], where redundancy is used for obstacle avoidance and [28], where the object dynamics is not taken into account; [29] and [30] propose protocols based on graph-based communication by neglecting parts of the overall system dynamics, and [18], [30] consider leader-follower approaches. An observer-based (for state and task estimation) adaptive control scheme is proposed in [24]. Model-based force-control control protocols with unilateral constraints are developed in [31], [32]. Formation control approaches are considered in [32], [33] and a navigation-function scheme is used in [34]; [35] includes hybrid control with intermittent contacts and in our previous work [36] we considered an MPC approach for the centralized cooperative object transportation. Finally, internal force and load distribution analysis in cooperative manipulation tasks is performed in a variety of works (e.g., [37]–[41]).

Note that most of the aforementioned adaptive control schemes (except e.g., [21]) employ the usual regressor matrix technique to compensate for unknown dynamic parameters [42], [43], which assumes a known structure of the dynamic terms. Such structures can be still difficult to obtain accurately though, especially when complex manipulators are considered. Moreover, in terms of load distribution, many of the related works use load sharing coefficients (e.g., [4], [5], [21]), without proving that undesired internal forces do not arise, or the standard Moore-Penrose inverse of the grasp matrix (e.g. [6], [17]), which has been questioned in [37].

A. Contribution and Outline

In this paper we propose two novel nonlinear control protocols for the trajectory tracking by the center of mass of an object that is rigidly grasped by N robotic agents, without using force/torque measurements at the grasping points.

Firstly, we develop a decentralized control scheme that combines the following attributes:

- 1) adaptation laws to compensate for external disturbances and uncertainties of the agents' and the object's dynamic parameters,
- 2) quaternion modeling of the object's orientation which avoids undesired representation singularities,
- 3) the load distribution proposed in [40] that provably avoids undesired internal forces,
- 4) validation through realistic simulations and real-time experiments.

The combination of unit quaternions and adaptive control for trajectory tracking in 2nd order dynamics renders the stability analysis a quite challenging procedure, due to the inherent topological limitations of stabilization on the unit sphere. The control scheme is an extension of our preliminary work [44], where a locally stabilizing adaptive quaternion-based controller had been used, without an appropriate internal force-free load distribution or experimental validation.

Secondly, we propose a decentralized control scheme that does not depend on the dynamic structure or parameters of the overall system and guarantees *predefined* transient and steady-state performance for the object's center of mass, using the Prescribed Performance Control scheme, initially proposed in [45], and used in single manipulation tasks in [46]–[48]. We have employed the specific scheme in our previous work [49] to design *timed* transition systems for a cooperatively manipulated object. In this work, however, we perform a more extended and detailed analysis by deriving specific bounds for the inputs of the robotic arms (i.e., joint velocities and torques), as well as real-time experiments.

The rest of the paper is organized as follows. Section II provides the notation used throughout the paper and necessary background. The modeling of the system as well as the problem formulation are given in Section III. Section IV presents the details of the two proposed control schemes with the corresponding stability analysis, and Section V illustrates the simulation and experimental results. Finally, Section VI concludes the paper.

II. NOTATION AND PRELIMINARIES

A. Notation

The set of positive integers is denoted by \mathbb{N} and the real n -coordinate space, with $n \in \mathbb{N}$, by \mathbb{R}^n ; $\mathbb{R}_{\geq 0}^n$ and $\mathbb{R}_{> 0}^n$ are the sets of real n -vectors with all elements nonnegative and positive, respectively. The $n \times n$ identity matrix is denoted by I_n , the n -dimensional zero vector by 0_n and the $n \times m$ matrix with zero entries by $0_{n \times m}$. Given a matrix $A \in \mathbb{R}^{n \times m}$, we use $\|A\| := \sqrt{\lambda_{\max}(A^T A)}$, where $\lambda_{\max}(\cdot)$ is the maximum eigenvalue of a matrix. The vector connecting the origins of coordinate frames $\{A\}$ and $\{B\}$ expressed in frame $\{C\}$ coordinates in 3-D space is denoted as $p_{B/A}^C \in \mathbb{R}^3$. Given $a \in \mathbb{R}^3$, $S(a)$ is the skew-symmetric matrix defined according to $S(a)b = a \times b$. The rotation matrix from $\{A\}$ to $\{B\}$ is denoted as $R_{B/A} \in SO(3)$, where $SO(3)$ is the 3-D rotation group. The angular velocity of frame $\{B\}$ with respect to $\{A\}$ is denoted as $\omega_{B/A} \in \mathbb{R}^3$ and it holds that [43] $\dot{R}_{B/A} = S(\omega_{B/A})R_{B/A}$. We further denote as $\eta_{A/B} \in \mathbb{T}$ the Euler angles representing the orientation of $\{B\}$ with respect to $\{A\}$, with $\mathbb{T} := (-\pi, \pi) \times (-\frac{\pi}{2}, \frac{\pi}{2}) \times (-\pi, \pi)$. We also define the set $\mathbb{M} := \mathbb{R}^3 \times \mathbb{T}$. In addition, S^n denotes the $(n+1)$ -dimensional sphere. For notational brevity, when a coordinate frame corresponds to an inertial frame of reference $\{I\}$, we will omit its explicit notation (e.g., $p_B = p_{B/I}^I, \omega_B = \omega_{B/I}^I, R_B = R_{B/I}$ etc.). Finally, all vector and matrix differentiations will be with respect to an inertial frame $\{I\}$, unless otherwise stated.

B. Unit Quaternions

Given two frames $\{A\}$ and $\{B\}$, we define a unit quaternion $\zeta_{B/A} := [\varphi_{B/A}, \epsilon_{B/A}^T]^T \in S^3$ describing the orientation of $\{B\}$ with respect to $\{A\}$, with $\varphi_{B/A} \in \mathbb{R}, \epsilon_{B/A} \in \mathbb{R}^3$, subject to the constraint $\varphi_{B/A}^2 + \epsilon_{B/A}^T \epsilon_{B/A} = 1$. The relation between $\zeta_{B/A}$ and the corresponding rotation matrix $R_{B/A}$ as well as the axis/angle representation can be found in [43]. For a given quaternion $\zeta_{B/A} = [\varphi_{B/A}, \epsilon_{B/A}^T]^T \in S^3$, its conjugate, that

corresponds to the orientation of $\{A\}$ with respect to $\{B\}$, is [43] $\zeta_{B/A}^+ = [\varphi_{B/A}, -\epsilon_{B/A}^\top]^\top \in S^3$. Moreover, given two quaternions $\zeta_i := \zeta_{B_i/A_i} = [\varphi_{B_i/A_i}, \epsilon_{B_i/A_i}^\top]^\top, \forall i \in \{1, 2\}$, the quaternion product is defined as [43]

$$\zeta_1 \otimes \zeta_2 = \begin{bmatrix} \varphi_1 \varphi_2 - \epsilon_1^\top \epsilon_2 \\ \varphi_1 \epsilon_2 + \varphi_2 \epsilon_1 + S(\epsilon_1) \epsilon_2 \end{bmatrix} \in S^3, \quad (1)$$

where $\varphi_i := \varphi_{B_i/A_i}, \epsilon_i := \epsilon_{B_i/A_i}, \forall i \in \{1, 2\}$.

For a moving frame $\{B\}$ (with respect to $\{A\}$), the time derivative of the quaternion $\zeta_{B/A} = [\varphi_{B/A}, \epsilon_{B/A}^\top]^\top \in S^3$ is given by [43]:

$$\dot{\zeta}_{B/A} = \frac{1}{2} E(\zeta_{B/A}) \omega_{B/A}^A, \quad (2a)$$

where $E : S^3 \rightarrow \mathbb{R}^{4 \times 3}$ is defined as:

$$E(\zeta) = \begin{bmatrix} -\epsilon^\top \\ \varphi I_3 - S(\epsilon) \end{bmatrix}, \forall \zeta = [\varphi, \epsilon^\top]^\top \in S^3.$$

Finally, it can be shown that $[E(\zeta)]^\top E(\zeta) = I_3, \forall \zeta \in S^3$ and hence (2a) implies

$$\omega_{B/A}^A = 2[E(\zeta_{B/A})]^\top \dot{\zeta}_{B/A}. \quad (2b)$$

It can be also shown that

$$\dot{\omega}_{B/A}^A = 2[E(\zeta_{B/A})]^\top \ddot{\zeta}_{B/A}. \quad (2c)$$

C. Prescribed Performance

Prescribed performance control, recently proposed in [45], describes the behavior where a tracking error $e : \mathbb{R}_{\geq 0} \rightarrow \mathbb{R}$ evolves strictly within a predefined region that is bounded by certain functions of time, achieving prescribed transient and steady state performance. The mathematical expression of prescribed performance is given by the following inequalities:

$$-\rho_L(t) < e(t) < \rho_U(t), \quad \forall t \in \mathbb{R}_{\geq 0},$$

where $\rho_L(t), \rho_U(t)$ are smooth and bounded decaying functions of time satisfying $\lim_{t \rightarrow \infty} \rho_L(t) > 0$ and $\lim_{t \rightarrow \infty} \rho_U(t) > 0$, called performance functions. Specifically, for the exponential performance functions $\rho_i(t) := (\rho_{i,0} - \rho_{i,\infty}) \exp(-l_i t) + \rho_{i,\infty}$, with $\rho_{i,0}, \rho_{i,\infty}, l_i \in \mathbb{R}_{>0}, i \in \{U, L\}$, appropriately chosen constants, the terms $\rho_{L,0} := \rho_L(0), \rho_{U,0} := \rho_U(0)$ are selected such that $\rho_{U,0} > e(0) > \rho_{L,0}$ and the terms $\rho_{L,\infty} := \lim_{t \rightarrow \infty} \rho_L(t), \rho_{U,\infty} := \lim_{t \rightarrow \infty} \rho_U(t)$ represent the maximum allowable size of the tracking error $e(t)$ at steady state, which may be set arbitrarily small to a value reflecting the resolution of the measurement device, thus achieving practical convergence of $e(t)$ to zero. Moreover, the decreasing rate of $\rho_L(t), \rho_U(t)$, which is affected by the constants l_L, l_U in this case, introduces a lower bound on the required speed of convergence of $e(t)$. Therefore, the appropriate selection of the performance functions $\rho_L(t), \rho_U(t)$ imposes performance characteristics on the tracking error $e(t)$.

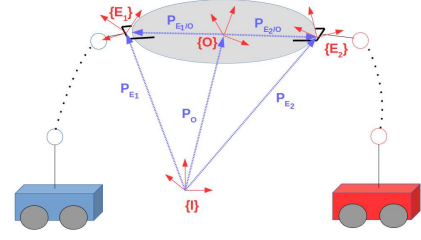


Fig. 1: Two robotic agents rigidly grasping an object.

D. Dynamical Systems

Consider the initial value problem:

$$\dot{\sigma} = H(\sigma, t), \sigma(0) \in \Omega, \quad (3)$$

with $H : \Omega \times \mathbb{R}_{\geq 0} \rightarrow \mathbb{R}^n$ where $\Omega \subset \mathbb{R}^n$ is a non-empty open set.

Definition 1. [50] A solution $\sigma(t)$ of the initial value problem (3) is maximal if it has no proper right extension that is also a solution of (3).

Theorem 1. [50] Consider problem (3). Assume that $H(\sigma, t)$ is: a) locally Lipschitz on σ for almost all $t \in \mathbb{R}_{\geq 0}$, b) piecewise continuous on t for each fixed $\sigma \in \Omega$ and c) locally integrable on t for each fixed $\sigma \in \Omega$. Then, there exists a maximal solution $\sigma(t)$ of (3) on $[0, t_{\max})$ with $t_{\max} > 0$ such that $\sigma(t) \in \Omega, \forall t \in [0, t_{\max})$.

Proposition 1. [50] Assume that the hypotheses of Theorem 1 hold. For a maximal solution $\sigma(t)$ on the time interval $[0, t_{\max})$ with $t_{\max} < \infty$ and for any compact set $\Omega' \subset \Omega$ there exists a time instant $t' \in [0, t_{\max})$ such that $\sigma(t') \notin \Omega'$.

III. PROBLEM FORMULATION

Consider N fully actuated robotic agents (e.g. robotic arms mounted on omnidirectional mobile bases) rigidly grasping an object (see Fig. 1). We denote by $\{E_i\}, \{O\}$ the end-effector and object's center of mass frames, respectively; $\{I\}$ corresponds to an inertial frame of reference, as mentioned in Section II-A. The rigidity assumption implies that the agents can exert both forces and torques along all directions to the object. In the following, we present the modeling of the coupled kinematics and dynamics of the object and the agents, which follows closely the one in [4], [6].

A. Robotic Agents

We denote by $q_i, \dot{q}_i \in \mathbb{R}^{n_i}$, with $n_i \in \mathbb{N}, \forall i \in \mathcal{N}$, the generalized joint-space variables and their time derivatives of agent i , with $q_i := [q_{i1}, \dots, q_{in_i}]$. Here, q_i consists of the degrees of freedom of the robotic arm as well as the moving base. The overall joint configuration is then $q := [q_1^\top, \dots, q_N^\top]^\top, \dot{q} := [\dot{q}_1^\top, \dots, \dot{q}_N^\top]^\top \in \mathbb{R}^n$, with $n := \sum_{i \in \mathcal{N}} n_i$. In addition, the inertial position and Euler-angle orientation of the i th end-effector, denoted by p_{E_i} and η_{E_i} , respectively, can be derived by the forward kinematics and are smooth functions of q_i , i.e. $p_{E_i} : \mathbb{R}^{n_i} \rightarrow \mathbb{R}^3, \eta_{E_i} : \mathbb{R}^{n_i} \rightarrow \mathbb{T}$. The generalized velocity of each agent's end-effector $v_i := [\dot{p}_{E_i}^\top, \omega_{E_i}^\top]^\top \in \mathbb{R}^6$, can be

computed through the differential kinematics $v_i = J_i(q_i)\dot{q}_i$ [43], where $J_i : \mathbb{R}^{n_i} \rightarrow \mathbb{R}^{6 \times n_i}$ is a smooth function representing the geometric Jacobian matrix, $\forall i \in \mathcal{N}$ [43]. The latter leads also to

$$\dot{v}_i = J_i(q_i)\ddot{q}_i + \dot{J}_i(q_i)\dot{q}_i. \quad (4)$$

We define also the set $\mathbb{S}_i := \{q_i \in \mathbb{R}^{n_i} : \det(J_i(q_i)J_i(q_i)^\top) > 0\}$ which contains all the singularity-free configurations. The differential equation describing the dynamics of each agent in task-space coordinates is [43]:

$$M_i(q_i)\dot{v}_i + C_i(q_i, \dot{q}_i)v_i + g_i(q_i) + d_i(q_i, \dot{q}_i, t) = u_i - f_i, \quad (5)$$

where $M_i : \mathbb{S}_i \rightarrow \mathbb{R}^{n_i \times n_i}$ is the positive definite inertia matrix, $C_i : \mathbb{S}_i \times \mathbb{R}^{n_i} \rightarrow \mathbb{R}^{n_i \times n_i}$ is the Coriolis matrix, $g_i : \mathbb{S}_i \rightarrow \mathbb{R}^{n_i}$ is the joint-space gravity term, $d_i : \mathbb{S}_i \times \mathbb{R}^{n_i} \times \mathbb{R}_{\geq 0} \rightarrow \mathbb{R}^{n_i}$ is a vector representing unmodeled friction, uncertainties and external disturbances, $f_i \in \mathbb{R}^6$ is the vector of generalized forces that agent i exerts on the grasping point with the object and $u_i \in \mathbb{R}^6$ is the task space wrench, that acts as the control input; u_i is related to the input torques τ_i via $\tau_i = J_i^\top(q_i)u_i + (I_{n_i} - J_i^\top(q_i)[J_i^+(q_i)]^\top)\tau_{i0}$, where J_i^+ is a generalized inverse of the manipulator Jacobian J_i [43]. Moreover, τ_{i0} concerns redundant agents ($n_i > 6$) and does not contribute to end-effector forces. The agent task-space dynamics (5) can be written in vector form as:

$$M(q)\dot{v} + C(q, \dot{q})v + g(q) + d(q, \dot{q}, t) = u - f, \quad (6)$$

where $v := [v_1^\top, \dots, v_N^\top] \in \mathbb{R}^{6N}$, $M := \text{diag}\{[M_i]_{i \in \mathcal{N}}\} \in \mathbb{R}^{6N \times 6N}$, $C := \text{diag}\{[C_i]_{i \in \mathcal{N}}\} \in \mathbb{R}^{6N \times 6N}$, $f := [f_1^\top, \dots, f_N^\top]^\top$, $u := [u_1^\top, \dots, u_N^\top]^\top$, $g := [g_1^\top, \dots, g_N^\top]^\top$, $d := [d_1^\top, \dots, d_N^\top]^\top \in \mathbb{R}^{6N}$.

B. Object

Regarding the object, we denote by $x_o := [p_o^\top, \eta_o^\top]^\top \in \mathbb{M}$, $v_o := [\dot{p}_o^\top, \omega_o^\top]^\top \in \mathbb{R}^{12}$ the pose and generalized velocity of its center of mass, which is considered as the object's state. We consider the following second order dynamics, which can be derived based on the Newton-Euler formulation:

$$\dot{x}_o = J_o(\eta_o)v_o, \quad (7a)$$

$$M_o(x_o)\dot{v}_o + C_o(x_o, \dot{x}_o)v_o + g_o(x_o) + d_o(x_o, \dot{x}_o, t) = f_o, \quad (7b)$$

where $M_o : \mathbb{M} \rightarrow \mathbb{R}^{6 \times 6}$ is the positive definite inertia matrix, $C_o : \mathbb{M} \times \mathbb{R}^6 \rightarrow \mathbb{R}^{6 \times 6}$ is the Coriolis matrix, $g_o : \mathbb{M} \rightarrow \mathbb{R}^6$ is the gravity vector, $d_o : \mathbb{M} \times \mathbb{R}^6 \times \mathbb{R}_{\geq 0} \rightarrow \mathbb{R}^6$ a vector representing modeling uncertainties and external disturbances, and $f_o \in \mathbb{R}^6$ is the vector of generalized forces acting on the object's center of mass. Moreover, $J_o : \mathbb{T} \rightarrow \mathbb{R}^{6 \times 6}$ is the object representation Jacobian $J_o(\eta_o) := \text{diag}\{I_3, J_{o_\eta}(\eta_o)\}$, where $J_{o_\eta} : \mathbb{T} \rightarrow \mathbb{R}^{3 \times 3}$:

$$J_{o_\eta}(\eta_o) := \begin{bmatrix} 1 & \sin(\phi_o) \tan(\theta_o) & \cos(\phi_o) \tan(\theta_o) \\ 0 & \cos(\phi_o) & -\sin(\theta_o) \\ 0 & \frac{\sin(\phi_o)}{\cos(\theta_o)} & \frac{\cos(\phi_o)}{\cos(\theta_o)} \end{bmatrix},$$

and is not well-defined when $\theta_o = \pm \frac{\pi}{2}$, which is referred to as *representation singularity*. Moreover, it can be proved that

$$\|J_o(\eta_o)\| = \sqrt{\frac{|\sin(\theta_o)|+1}{1-\sin^2(\theta_o)}}, \quad (8a)$$

$$\|J_o(\eta_o)^{-1}\| = \sqrt{1 + \sin(\theta_o)} \leq \sqrt{2}, \quad (8b)$$

where $J_o(\cdot)^{-1}$ is the matrix inverse.

A possible way to avoid the aforementioned singularity is to transform the Euler angles to a unit quaternion representation for the orientation. Hence, the term η_o can be transformed to the unit quaternion $\zeta_o = [\varphi_o, \epsilon_o^\top]^\top \in S^3$ [43], for which, following Section II-B and (2), one obtains:

$$\begin{aligned} \dot{\zeta}_o &= \frac{1}{2}E(\zeta_o)\omega_o \\ \omega_o &= 2[E(\zeta_o)]^\top \dot{\zeta}_o, \end{aligned}$$

which constitutes a singularity-free representation.

C. Coupled Dynamics

In view of Fig. 1, one concludes that the pose of the agents and the object's center of mass are related as

$$p_{E_i}(q_i) = p_o + p_{E_i/o}(q_i) = p_o + R_{E_i}(q_i)p_{E_i/o}^{E_i}, \quad (9a)$$

$$\eta_{E_i}(q_i) = \eta_o + \eta_{E_i/o}, \quad (9b)$$

$\forall i \in \mathcal{N}$, where $p_{E_i/o}^{E_i}$ and $\eta_{E_i/o}$ are the *constant* distance and orientation offset vectors between $\{O\}$ and $\{E_i\}$. Following (9), along with the fact that, due to the grasping rigidity, it holds that $\omega_{E_i} = \omega_o, \forall i \in \mathcal{N}$, one obtains

$$v_i = J_{o_i}(q_i)v_o, \quad (10)$$

where $J_{o_i} : \mathbb{R}^{n_i} \rightarrow \mathbb{R}^{6 \times 6}$ is the object-to-agent Jacobian matrix, with

$$J_{o_i}(x) = \begin{bmatrix} I_3 & S(p_{o/E_i}(x)) \\ 0_{3 \times 3} & I_3 \end{bmatrix}, \forall x \in \mathbb{R}^{n_i}, \quad (11)$$

which is always full-rank. Moreover, from (10), one obtains

$$\dot{v}_i = J_{o_i}(q_i)\dot{v}_o + \dot{J}_{o_i}(q_i)v_o. \quad (12)$$

In addition, it can be proved for J_{o_i} that

$$\|J_{o_i}(x)\| \leq \|p_{o/E_i}^{E_i}\| + 1, \forall x \in \mathbb{R}^{n_i}, i \in \mathcal{N}, \quad (13)$$

which will be used in the subsequent analysis.

The kineto-statics duality along with the grasp rigidity suggest that the force f_o acting on the object's center of mass and the generalized forces $f_i, i \in \mathcal{N}$, exerted by the agents at the grasping points, are related through:

$$f_o = [G(q)]^\top f, \quad (14)$$

where $G : \mathbb{R}^n \rightarrow \mathbb{R}^{6N \times 6}$, with $G(q) := [[J_{o_1}(q_1)]^\top, \dots, [J_{o_N}(q_N)]^\top]^\top$, is the full column-rank grasp matrix. By substituting (6) into (14), we obtain:

$$f_o = [G(q)]^\top (u - M(q)\dot{v} - C(q, \dot{q})v - g(q) - d(q, \dot{q}, t)),$$

which, after substituting (10), (12), (7), and rearranging terms, yields the overall system coupled dynamics:

$$\tilde{M}(x)\dot{v}_o + \tilde{C}(x)v_o + \tilde{g}(x) + \tilde{d}(x, t) = [G(q)]^\top u, \quad (15)$$

where

$$\widetilde{M}(x) := M_o(x_o) + [G(q)]^\top M(q)G(q) \quad (16a)$$

$$\begin{aligned} \widetilde{C}(x) := & C_o(x_o, \dot{x}_o) + [G(q)]^\top C(q, \dot{q})G(q) \\ & + [G(q)]^\top M(q)\dot{G}(q) \end{aligned} \quad (16b)$$

$$\widetilde{g}(x) := g_o(x_o) + [G(q)]^\top g(q). \quad (16c)$$

$$\begin{aligned} \widetilde{d}(x, t) := & d_o(x_o, \dot{x}_o, t) + [G(q)]^\top d(q, \dot{q}, t) \\ & (16d) \end{aligned} \quad (16e)$$

and x is the overall state $x := [q^\top, \dot{q}^\top, x_o^\top, \dot{x}_o^\top]^\top \in \mathbb{S} \times \mathbb{R}^{n+6} \times \mathbb{M}, \mathbb{S} := \mathbb{S}_1 \times \dots \times \mathbb{S}_N$. Moreover, the following Lemma, whose proof can be found in [44], is necessary for the following analysis.

Lemma 1. *The matrix $\widetilde{M}(x)$ is symmetric and positive definite and the matrix $\widetilde{M}(x) - 2\widetilde{C}(x)$ is skew symmetric, i.e.,*

$$\begin{aligned} \left[\widetilde{M}(x) - 2\widetilde{C}(x) \right]^\top &= - \left[\widetilde{M}(x) - 2\widetilde{C}(x) \right], \forall x \in \mathbb{R}^6 \\ y^\top \left[\widetilde{M}(x) - 2\widetilde{C}(x) \right] y &= 0, \quad \forall x, y \in \mathbb{R}^6. \end{aligned}$$

The positive definiteness of $\widetilde{M}(x)$ leads to the property

$$\underline{m}I_6 \leq \widetilde{M}(x) \leq \bar{m}I_6, \quad (17)$$

$\forall x \in \mathbb{R}^{2n+6} \times \mathbb{R}$, where \underline{m} and \bar{m} are positive unknown constants.

We are now ready to state the problem treated in this paper:

Problem 1. *Given a desired bounded object smooth pose trajectory specified by $\bar{x}_d(t) := [(p_d(t))^\top, (\eta_d(t))^\top]^\top, p_d(t) \in \mathbb{R}^3, \eta_d(t) := [\varphi_d(t), \theta_d(t), \psi_d(t)] \in \mathbb{T}$, with bounded first and second derivatives, and $\theta_d(t) \in [-\bar{\theta}, \bar{\theta}] \subset (-\frac{\pi}{2}, \frac{\pi}{2}), \forall t \in \mathbb{R}_{\geq 0}$, as well as $v_o(0) = 0_6$, determine a continuous time-varying control law u in (15) such that*

$$\lim_{t \rightarrow \infty} \begin{bmatrix} p_o(t) \\ \eta_o(t) \end{bmatrix} = \begin{bmatrix} p_d(t) \\ \eta_d(t) \end{bmatrix}.$$

The requirement $\theta_d(t) \in [-\bar{\theta}, \bar{\theta}] \subset (-\frac{\pi}{2}, \frac{\pi}{2}), \forall t \in \mathbb{R}_{\geq 0}$ is a necessary condition needed to ensure that tracking of θ_d will not result in singular configurations of $J_o(\eta_o)$, which is needed for the control protocol of Section IV-B. The constant $\bar{\theta} \in [0, \frac{\pi}{2})$ can be taken arbitrarily close to $\frac{\pi}{2}$.

To solve the aforementioned problem, we need the following assumptions regarding the agent feedback, the bounds of the uncertainties/disturbances, and the kinematic singularities.

Assumption 1 (Feedback). *Each agent $i \in \mathcal{N}$ has continuous feedback of its own state q_i, \dot{q}_i .*

Assumption 2 (Object Geometry). *Each agent $i \in \mathcal{N}$ knows the constant offsets $p_{E_i/O}^{E_i}$ and $\eta_{E_i/O}, \forall i \in \mathcal{N}$.*

Assumption 3 (Kinematic Singularities). *The robotic agents operate away from kinematic singularities, i.e., $q_i \in \mathbb{S}_i, \forall i \in \mathcal{N}$.*

Assumption 1 is realistic for real manipulation systems, since on-board sensor can provide accurately the measurements q_i, \dot{q}_i . The object geometric characteristics in Assump-

tion 2 can be obtained by on-board sensors, whose inaccuracies are not modeled here and constitute part of future work. Finally, Assumption 3 states that the q_i that achieve $x_o(t) = \bar{x}_d(t), \forall t \in \mathbb{R}_{\geq 0}$ are sufficiently far from singular configurations.

Since each agent has feedback from its state q_i, \dot{q}_i , it can compute through the forward and differential kinematics the end-effector pose $p_{E_i}(q_i), \eta_{E_i}(q_i)$ and the velocity $v_i, \forall i \in \mathcal{N}$. Moreover, since it knows $p_{E_i/O}^{E_i}$ and $\eta_{E_i/O}$, it can compute $J_{o_i}(q_i)$ from (11), and x_o, v_o by inverting (9) and (10), respectively. Consequently, each agent can then compute the object unit quaternion ζ_o as well as $\dot{\zeta}_o$.

IV. MAIN RESULTS

In this section we present two control schemes for the solution of Problem 1. The proposed controllers are decentralized, in the sense that the agents calculate their control signal on their own, without communicating with each other, as well as robust, since they do not take into account the dynamic properties of the agents or the object (mass/inertia moments) or the uncertainties/external disturbances modeled by the function $\widetilde{d}(x, t)$ in (15). The first control scheme is presented in Section IV-A, and is based on quaternion feedback and adaptation laws, while the second control scheme is given in Section IV-B and is inspired by the Prescribed Performance Control (PPC) Methodology introduced in [45].

A. Adaptive Control with Quaternion Feedback

The proposed controller of this section follows closely the adaptive control methodology of [42]. Firstly, we need the following assumption regarding the model uncertainties/external disturbances.

Assumption 4 (Uncertainties/Disturbance parameterization). *There exist constant unknown vectors $\bar{d}_o \in \mathbb{R}^{\mu_o}, \bar{d}_i \in \mathbb{R}^\mu$ and known bounded functions $\delta_o : \mathbb{M} \times \mathbb{R}^6 \times \mathbb{R}_{\geq 0} \rightarrow \mathbb{R}^{6 \times \mu_o}, \delta_i : \mathbb{R}^{2n_i} \times \mathbb{R}_{\geq 0} \rightarrow \mathbb{R}^{6 \times \mu}$, such that*

$$\begin{aligned} d_o(x_o, \dot{x}_o, t) &= \delta_o(x_o, \dot{x}_o, t)\bar{d}_o, \\ d_i(q_i, \dot{q}_i, t) &= \delta_i(q_i, \dot{q}_i, t)\bar{d}_i, \end{aligned}$$

$$\forall q_i, \dot{q}_i \in \mathbb{R}^{n_i}, x_o \in \mathbb{M}, \dot{x}_o \in \mathbb{R}^6, t \in \mathbb{R}_{\geq 0}, i \in \mathcal{N}.$$

For real applications, the function δ, δ_i in the aforementioned assumption can be approximated using neural networks and learning techniques. Without loss of generality, we have also assumed that μ is the same for all agents.

The desired Euler angle orientation vector $\eta_d : \mathbb{R}_{\geq 0} \rightarrow \mathbb{T}$ is transformed first to the unit quaternion $\zeta_d : \mathbb{R}_{\geq 0} \rightarrow S^3$ [43]. Then, we need to define the errors associated with the object pose and the desired pose trajectory. We first define the state that corresponds to the position error:

$$e_p := p_o - p_d(t).$$

Since unit quaternions do not form a vector space, they cannot be subtracted to form an orientation error; instead we should use the properties of the quaternion group algebra. Let

$e_\zeta = [e_\varphi, e_\epsilon^\top]^\top \in S^3$ be the unit quaternion describing the orientation error. Then, it holds that [43],

$$e_\zeta = \zeta_d(t) \otimes \zeta_o^+ = \begin{bmatrix} \varphi_d(t) \\ \epsilon_d(t) \end{bmatrix} \otimes \begin{bmatrix} \varphi_o \\ -\epsilon_o \end{bmatrix},$$

which, by using (1), becomes:

$$e_\zeta = \begin{bmatrix} e_\varphi \\ e_\epsilon \end{bmatrix} := \begin{bmatrix} \varphi_o \varphi_d(t) + \epsilon_o^\top \epsilon_d(t) \\ \varphi_o \epsilon_d(t) - \varphi_d(t) \epsilon_o + S(\epsilon_o) \epsilon_d(t) \end{bmatrix}. \quad (18)$$

By employing (2) and certain properties of skew-symmetric matrices [51], it can be shown that the error dynamics of e_p, e_φ are:

$$\dot{e}_p = \dot{p}_o - \dot{p}_d(t) \quad (19a)$$

$$\dot{e}_\varphi = \frac{1}{2} e_\epsilon^\top e_\omega \quad (19b)$$

$$\dot{e}_\epsilon = -\frac{1}{2} [e_\varphi I_3 + S(e_\epsilon)] e_\omega - S(e_\epsilon) \omega_d(t), \quad (19c)$$

where $e_\omega := \omega_o - \omega_d(t)$ is a state for the angular velocity error, with $\omega_d(t) = 2[E(\zeta_d(t))]^\top \dot{\zeta}_d(t)$, as indicated by (2b).

Due to the ambiguity of unit quaternions, when $\zeta_o = \zeta_d$, then $e_\zeta = [1, 0_3^\top]^\top \in S^3$. If $\zeta_o = -\zeta_d$, then $e_\zeta = [-1, 0_3^\top]^\top \in S^3$, which, however, represents the same orientation. Therefore, the control objective established in Problem 1 is equivalent to

$$\lim_{t \rightarrow \infty} \begin{bmatrix} e_p(t) \\ |e_\varphi(t)| \\ e_\epsilon(t) \end{bmatrix} = \begin{bmatrix} 0_3 \\ 1 \\ 0_3 \end{bmatrix}.$$

The left hand side of (5), after employing (10) and (12), becomes

$$\begin{aligned} M_i(q_i) \dot{v}_i + C_i(q_i, \dot{q}_i) v_i + g_i(q_i) + d_i(q_i, \dot{q}_i, t) = \\ M_i(q_i) \left(J_{o_i}(q_i) \dot{v}_o + \dot{J}_{o_i}(q_i) v_o \right) + C_i(q_i, \dot{q}_i) J_{o_i}(q_i) v_o + \\ g_i(q_i) + d_i(q_i, \dot{q}_i, t). \end{aligned}$$

which, according to Assumption 4 and the fact that the manipulator dynamics can be linearly parameterized with respect to dynamic parameters [42], becomes

$$\begin{aligned} M_i(q_i) J_{o_i}(q_i) \dot{v}_o + \left(M_i(q_i) \dot{J}_{o_i}(q_i) + C_i(q_i, \dot{q}_i) J_{o_i}(q_i) \right) v_o \\ + g_i(q_i) + d_i(q_i, \dot{q}_i, t) = Y_i(q_i, \dot{q}_i, v_o, \dot{v}_o) \vartheta_i + \delta_i(q_i, \dot{q}_i, t) \bar{d}_i, \end{aligned} \quad (20a)$$

$\forall i \in \mathcal{N}$, where $\vartheta_i \in \mathbb{R}^\ell$, $\ell \in \mathbb{N}$, are vectors of unknown but constant dynamic parameters of the agents, appearing in the terms M_i, C_i, g_i , and $Y_i : \mathbb{R}^{2n_i+12} \rightarrow \mathbb{R}^{6 \times \ell}$ are known regressor matrices, independent of $\vartheta_i, i \in \mathcal{N}$. Without loss of generality, we assume here that the dimension of ϑ_i is the same, ℓ for all the agents. Similarly, the dynamical terms of the left hand side of (7b) can be written as

$$\begin{aligned} M_o(x_o) \dot{v}_o + C_o(x_o, \dot{x}_o) v_o + g_o(x_o) + d_o(x_o, \dot{x}_o, t) \\ = Y_o(x_o, \dot{x}_o, v_o, \dot{v}_o) \vartheta_o + \delta_o(x_o, \dot{x}_o, t) \bar{d}_o, \end{aligned} \quad (20b)$$

where $\vartheta_o \in \mathbb{R}^{\ell_o}$, $\ell_o \in \mathbb{N}$ is a vector of unknown but constant dynamic parameters of the object, appearing in the terms M_o, C_o, g_o , and $Y_o : \mathbb{M} \times \mathbb{R}^{18} \rightarrow \mathbb{R}^{6 \times \ell_o}$ is a known regressor matrix, independent of ϑ_o . It is worth noting that the choice for ℓ and ℓ_o is not unique.

Hence, in view of (16) and (20), the left-hand side of (15) can be written as:

$$\begin{aligned} \widetilde{M}(x) \dot{v}_o + \widetilde{C}(x) v_o + \widetilde{g}(x) + \widetilde{d}(x, t) = Y_o(x_o, \dot{x}_o, v_o, \dot{v}_o) \vartheta_o \\ + \delta_o(x_o, \dot{x}_o, t) \bar{d}_o + [G(q)]^\top \left(\widetilde{Y}(q, \dot{q}, v_o, \dot{v}_o) \vartheta + \widetilde{\delta}(q, \dot{q}, t) \bar{d} \right), \end{aligned} \quad (21)$$

where $\vartheta := [\vartheta_1^\top, \dots, \vartheta_N^\top]^\top \in \mathbb{R}^{N\ell}$, $\widetilde{Y}(q, \dot{q}, v_o, \dot{v}_o) := \text{diag}\{[Y_i(q_i, \dot{q}_i, v_o, \dot{v}_o)]_{i \in \mathcal{N}}\} \in \mathbb{R}^{6N \times N\ell}$, $\widetilde{\delta}(q, \dot{q}, t) := \text{diag}\{[\delta_i(q_i, \dot{q}_i, t)]_{i \in \mathcal{N}}\} \in \mathbb{R}^{6N \times N\mu}$, and $\bar{d} := [\bar{d}_1^\top, \dots, \bar{d}_N^\top]^\top \in \mathbb{R}^{N\mu}$.

Let us now introduce the states $\hat{\vartheta}_o \in \mathbb{R}^{\ell_o}$ and $\hat{\vartheta}_i \in \mathbb{R}^\ell$ which represent the estimates of ϑ_o and ϑ_i , respectively, by agent $i \in \mathcal{N}$, and the corresponding stack vector $\hat{\vartheta} := [\hat{\vartheta}_1^\top, \dots, \hat{\vartheta}_N^\top]^\top \in \mathbb{R}^{N\ell}$, for which we formulate the associated errors as

$$e_{\vartheta_o} := \vartheta_o - \hat{\vartheta}_o \in \mathbb{R}^{\ell_o} \quad (22a)$$

$$e_{\vartheta} := \begin{bmatrix} e_{\vartheta_1} \\ \vdots \\ e_{\vartheta_N} \end{bmatrix} := \begin{bmatrix} \vartheta_1 - \hat{\vartheta}_1 \\ \vdots \\ \vartheta_N - \hat{\vartheta}_N \end{bmatrix} = \vartheta - \hat{\vartheta} \in \mathbb{R}^{N\ell}. \quad (22b)$$

In the same vein, we introduce the states $\hat{d}_o \in \mathbb{R}^{\mu_o}$ and $\hat{d}_i \in \mathbb{R}^\mu$ that correspond to the estimates of \bar{d}_o and \bar{d}_i , respectively, by agent $i \in \mathcal{N}$, and the corresponding stack vector $\hat{d} := [\hat{d}_1, \dots, \hat{d}_N]^\top \in \mathbb{R}^{N\mu}$, for which we also formulate the associated errors as

$$e_{d_o} := \bar{d}_o - \hat{d}_o \in \mathbb{R}^{\mu_o} \quad (23a)$$

$$e_d := \begin{bmatrix} e_{d_1} \\ \vdots \\ e_{d_N} \end{bmatrix} := \begin{bmatrix} \bar{d}_1 - \hat{d}_1 \\ \vdots \\ \bar{d}_N - \hat{d}_N \end{bmatrix} = \bar{d} - \hat{d} \in \mathbb{R}^{N\mu}. \quad (23b)$$

Next, we design the reference velocity

$$v_f := v_d(t) - K_f e = \begin{bmatrix} \dot{p}_d(t) - k_p e_p \\ \omega_d(t) + k_\zeta e_\epsilon \end{bmatrix} \quad (24)$$

with $K_f := \text{diag}\{k_p, k_\zeta\}$, $e := [e_p^\top, -e_\epsilon^\top]^\top \in \mathbb{R}^6$, k_p, k_ζ positive control gains. We also introduce the respective velocity error e_v as

$$e_{v_f} := v_o - v_f, \quad (25)$$

and design the adaptive control law u_i in (15), for each agent $i \in \mathcal{N}$, as:

$$\begin{aligned} u_i = Y_i(q_i, \dot{q}_i, v_f, \dot{v}_f) \hat{\vartheta}_i + \delta_i(q_i, \dot{q}_i, t) \hat{d}_i + \\ J_{M_i}(q) \left[Y_o(x_o, \dot{x}_o, v_f, \dot{v}_f) \hat{\vartheta}_o + \delta_o(x_o, \dot{x}_o, t) \hat{d}_o \right. \\ \left. - e - K_v e_{v_f} \right], \end{aligned} \quad (26)$$

where K_v is a diagonal positive definite gain matrix, and $J_{M_i} : \mathbb{R}^n \rightarrow \mathbb{R}^{6 \times 6}$ is the matrix [40]

$$J_{M_i}(q) := \begin{bmatrix} m_i^* [m_o^*]^{-1} I_3 & m_i^* [J_o^*(q)]^{-1} S(p_{o/E_i}(q_i)) \\ 0_{3 \times 3} & J_i^* [J_o^*(q)]^{-1} \end{bmatrix} \quad (27)$$

for some positive coefficients $m_i^* \in \mathbb{R}_{>0}$ and positive definite matrices $J_i^* \in \mathbb{R}^{3 \times 3}$, $\forall i \in \mathcal{N}$, satisfying

$$\begin{aligned} m_o^* &= \sum_{i \in \mathcal{N}} m_i^*, \\ J_o^*(q) &= \sum_{i \in \mathcal{N}} J_i^* - \sum_{i \in \mathcal{N}} m_i^* [S(p_{o/E_i}(q_i))]^2, \\ \sum_{i \in \mathcal{N}} p_{o/E_i}(q_i) m_i^* &= 0_3. \end{aligned}$$

In addition, we design the following adaptation laws:

$$\dot{\hat{\theta}}_i = -\gamma_i \left[Y_i(q_i, \dot{q}_i, v_f, \dot{v}_f) \right]^\top J_{o_i}(q_i) e_{v_f} \quad (28a)$$

$$\dot{\hat{\theta}}_o = -\gamma_o \left[Y_o(x_o, \dot{x}_o, v_f, \dot{v}_f) \right]^\top e_{v_f} \quad (28b)$$

$$\dot{\hat{d}}_i = -\beta_i [\delta_i(q_i, \dot{q}_i, t)]^\top J_{o_i}(q_i) e_{v_f} \quad (28c)$$

$$\dot{\hat{d}}_o = -\beta_o [\delta_o(x_o, \dot{x}_o, t)]^\top e_{v_f}, \quad (28d)$$

with arbitrary bounded initial conditions, where $\beta_i, \beta_o, \gamma_i, \gamma_o \in \mathbb{R}_{>0}$ are positive gains, $\forall i \in \mathcal{N}$. The control and adaptation laws can be written in vector form

$$\begin{aligned} u &= \tilde{Y}(q, \dot{q}, v_o, \dot{v}_o) \hat{\vartheta} + \tilde{\delta}(q, \dot{q}, t) \hat{d} + \\ G_M^+(q) &\left[Y_o(x_o, \dot{x}_o, v_f, \dot{v}_f) \hat{\vartheta}_o + \delta_o(x_o, \dot{x}_o, t) \hat{d}_o \right. \\ &\left. - e - K_v e_{v_f} \right] \end{aligned} \quad (29a)$$

$$\dot{\hat{\vartheta}} = -\Gamma [\tilde{Y}(q, \dot{q}, v_f, \dot{v}_f)]^\top G(q) e_{v_f} \quad (29b)$$

$$\dot{\hat{d}} = -B [\tilde{\delta}(q, \dot{q}, t)]^\top G(q) e_{v_f} \quad (29c)$$

$$\dot{\hat{\theta}}_o = -\gamma_o \left[Y_o(x_o, \dot{x}_o, v_f, \dot{v}_f) \right]^\top e_{v_f} \quad (29d)$$

$$\dot{\hat{d}}_o = -\beta_o [\delta_o(x_o, \dot{x}_o, t)]^\top e_{v_f}, \quad (29e)$$

where $G_M^+(q) := [J_{M_1}^\top(q), \dots, J_{M_N}^\top(q)]^\top \in \mathbb{R}^{6N \times 6}$, $B := \text{diag}\{[\beta_i]_{i \in \mathcal{N}}\}$, and $\Gamma := \text{diag}\{[\gamma_i]_{i \in \mathcal{N}}\}$. The matrix $G_M^+(q)$ was introduced in [40], where it was proved that it yields a load distribution that is free of internal forces. The parameters m_o^*, m_i^* are used to distribute the object's needed effort (in our case, the term that right multiplies $G_M^+(q)$ in (29a) to the agents.

Remark 1 (Decentralized manner (adaptive controller)).

Notice from (26),(28) that the overall control protocol is decentralized in the sense that the agents can calculate their own control signals without communicating with each other. In particular, the control gains and the desired trajectory can be transmitted off-line to the agents, which can compute the object's pose and velocity, and hence the signals e , v_f , e_{v_f} from the inverse kinematics. For the computation of $J_{M_i}(q)$, each agent needs feedback from all q_i to compute $S(p_{o/E_i}(q_i))$, $\forall i \in \mathcal{N}$. However, by exploiting the rigidity of the grasps, it holds that $p_{o/E_i}(q_i) = R_o(q_i) p_{o/E_i}^o$. Therefore, since all agents can compute R_o , the computation of $J_{M_i}(q)$ reduces to knowledge of the offsets p_{o/E_i}^o , which can also be transmitted off-line to the agents. Moreover, by also transmitting off-line to the agents the initial conditions $\hat{\theta}_o$, \hat{d}_o , and via the adaptation laws (29d), (29e), each agent has access to the adaptation signals $\hat{\theta}_o(t)$, $\hat{d}_o(t)$, $\forall t \in \mathbb{R}_{\geq 0}$. Finally,

the structure of the functions δ_i , δ_o , Y_i , Y_o , as well as the constants m_i^* , J_i^* can be also known by the agents a priori.

Theorem 2. Consider N robotic agents rigidly grasping an object with coupled dynamics described by (15) and unknown dynamic parameters. Then, under Assumptions 1-4, by applying the control protocol (26) with the adaptation laws (28), the object pose converges asymptotically to the desired pose trajectory. Moreover, all closed loop signals are bounded.

Proof: Consider the nonnegative function

$$\begin{aligned} V &:= \frac{1}{2} e_p^\top e_p + 2(1 - e_\varphi) + \frac{1}{2} e_{v_f}^\top \tilde{M}(x) e_{v_f} + \frac{1}{2} e_\vartheta^\top \Gamma^{-1} e_\vartheta + \\ &+ \frac{1}{2\gamma_o} e_{\vartheta_o}^\top e_{\vartheta_o} + \frac{1}{2} e_d^\top B^{-1} e_d + \frac{1}{2\beta_o} e_{d_o}^\top e_{d_o}, \end{aligned} \quad (30)$$

Recall that the error quaternion e_ζ as defined (18) is a unit quaternion and hence $e_\varphi \in [-1, 1]$.

By taking the derivative of V , we obtain

$$\begin{aligned} \dot{V} &= e^\top (v_o - v_d(t)) + \frac{1}{2} e_{v_f}^\top \dot{\tilde{M}}(x) e_{v_f} - e_{v_f}^\top \tilde{M}(x) \dot{v}_f \\ &+ e_{v_f}^\top \left([G(q)]^\top u - \tilde{C}(x) v_o - \tilde{g}(x) - \tilde{d}(x, t) \right) - e_\vartheta^\top \Gamma^{-1} \dot{\vartheta} \\ &- \frac{1}{\gamma_o} e_{\vartheta_o}^\top \dot{\vartheta}_o - e_d^\top B^{-1} \dot{d} - \frac{1}{\beta_o} e_{d_o}^\top \dot{d}_o, \end{aligned}$$

which, by using (25) and (24), becomes

$$\begin{aligned} \dot{V} &= -e^\top K_f e + \frac{1}{2} e_{v_f}^\top \dot{\tilde{M}}(x) e_{v_f} - e_{v_f}^\top \tilde{C}(x) e_{v_f} + \\ &e_{v_f}^\top \left([G(q)]^\top u + e - \tilde{M}(x) \dot{v}_f - \tilde{g}(x) - \tilde{C}(x) v_f - \tilde{d}(x, t) \right) \\ &- e_\vartheta^\top \Gamma^{-1} \dot{\vartheta} - \frac{1}{\gamma_o} e_{\vartheta_o}^\top \dot{\vartheta}_o - e_d^\top B^{-1} \dot{d} - \frac{1}{\beta_o} e_{d_o}^\top \dot{d}_o. \end{aligned}$$

By employing Lemma 1 as well as (21), \dot{V} can be written as

$$\begin{aligned} \dot{V} &= -e^\top K_f e + e_{v_f}^\top \left[[G(q)]^\top \left(u - \tilde{Y}(q, \dot{q}, v_f, \dot{v}_f) \vartheta - \right. \right. \\ &\left. \left. \tilde{\delta}(q, \dot{q}, t) \hat{d} \right) + e - Y_o(x_o, \dot{x}_o, \dot{v}_f, \dot{v}_f) \vartheta_o - \delta_o(x_o, \dot{x}_o, t) \hat{d}_o \right. \\ &\left. - e_\vartheta^\top \Gamma^{-1} \dot{\vartheta} - \frac{1}{\gamma_o} e_{\vartheta_o}^\top \dot{\vartheta}_o - e_d^\top B^{-1} \dot{d} - \frac{1}{\beta_o} e_{d_o}^\top \dot{d}_o \right], \end{aligned}$$

and after substituting the adaptive control and adaptation laws (29) and using the fact that $[G(q)]^\top G_M^+ = I_6$,

$$\begin{aligned} \dot{V} &= -e^\top K_f e - e_{v_f}^\top K_v e_{v_f} - \\ &e_{v_f}^\top \left[[G(q)]^\top \left(\tilde{Y}(q, \dot{q}, v_f, \dot{v}_f) e_\vartheta + \tilde{\delta}(q, \dot{q}, t) e_d \right) + \right. \\ &Y_o(x_o, \dot{x}_o, v_f, \dot{v}_f) e_{\vartheta_o} + \delta_o(x_o, \dot{x}_o, t) e_{d_o} \left. \right] + \\ &e_\vartheta^\top [\tilde{Y}(q, \dot{q}, v_f, \dot{v}_f)]^\top G(q) e_{v_f} + e_d^\top [\tilde{\delta}(q, \dot{q}, t)]^\top e_{v_f} + \\ &e_{\vartheta_o}^\top [Y_o(x_o, \dot{x}_o, v_f, \dot{v}_f)]^\top e_{v_f} + e_{d_o}^\top [\delta_o(x_o, \dot{x}_o, t)]^\top e_{v_f}, \end{aligned}$$

which becomes

$$\begin{aligned} \dot{V} &= -e^\top K_f e - e_{v_f}^\top K_v e_{v_f} \\ &= -k_p \|e_p\|^2 - k_\zeta \|e_\zeta\|^2 - e_{v_f}^\top K_v e_{v_f}, \end{aligned}$$

which is non-positive. We conclude therefore the boundedness of V and of χ , which implies the boundedness of the dynamic terms $\tilde{M}(x)$, $\tilde{C}(x)$, $\tilde{g}(x)$. Moreover, by invoking the boundedness of $p_d(t)$, $v_d(t)$, $\omega_d(t)$, $\dot{v}_d(t)$, $\dot{\omega}_d(t)$, we conclude the boundedness of v_f , v_o , v_i , ϑ_o , ϑ , \hat{d} , \hat{d}_o . By differentiating (19), we also conclude the boundedness of \dot{v}_f and therefore, the boundedness of the control and adaptation laws (26) and

(28). Thus, we can conclude the boundedness of the second derivative \ddot{V} and hence the uniform continuity of \dot{V} . By invoking Barbalat's lemma [52], we deduce therefore that $\lim_{t \rightarrow \infty} \dot{V}(t) = 0$ and, consequently, that $\lim_{t \rightarrow \infty} e_p(t) = 0_3$, $\lim_{t \rightarrow \infty} e_{v_f}(t) = 0_6$, and $\lim_{t \rightarrow \infty} \|e_\epsilon(t)\|^2 = 0$, which, given that e_ζ is a unit quaternion, leads to the configuration $(e_p, e_{v_f}, e_\varphi, e_\epsilon) = (0_3, 0_6, \pm 1, 0_3)$. ■

Remark 2 (Unwinding). Note that the two configurations where $e_\varphi = 1$ and $e_\varphi = -1$, respectively, represent the same orientation. The closed loop dynamics of e_φ , as given in (19b), can be written, in view of (24), as $\dot{e}_\varphi = k_\zeta \frac{1}{2} \|e_\epsilon\|^2 + \frac{1}{2} [0_3^\top, e_\epsilon^\top] e_{v_f}$. Since the first term is always positive, we conclude that the equilibrium point $(e_p, e_{v_f}, e_\varphi, e_\epsilon) = (0_3, 0_6, -1, 0_3)$ is unstable. Therefore, there might be trajectories close to the configuration $e_\varphi = -1$ that will move away and approach $e_\varphi = 1$, i.e., a full rotation will be performed to reach the desired orientation (of course, if the system starts at the equilibrium $(e_p, e_{v_f}, e_\varphi, e_\epsilon) = (0_3, 0_6, -1, 0_3)$, it will stay there, which also corresponds to the desired orientation behavior). This is the so-called unwinding phenomenon [53]. Note, however, that the desired equilibrium point $(e_p, e_{v_f}, e_\varphi, e_\epsilon) = (0_3, 0_6, 1, 0_3)$ is **eventually attractive**, meaning that for each $\delta_\epsilon > 0$, there exist finite a time instant $T \geq 0$ such that $1 - e_\varphi(t) < \delta_\epsilon, \forall t > T \geq 0$. A similar behavior is observed if we stabilize the point $e_\varphi = -1$ instead of $e_\varphi = 1$, by setting $e := [e_p^\top, e_\epsilon^\top]^\top$ in (24) and considering the term $2(1+e_\varphi)$ instead of $2(1-e_\varphi)$ in the Lyapunov function (30).

In order to avoid the unwinding phenomenon, instead of the error $e = [e_p^\top, -e_\epsilon^\top]^\top$, we can instead choose $e = [e_p^\top, -e_\varphi e_\epsilon^\top]^\top$ (see our preliminary result [44]). Then by considering the Lyapunov function

$$V = \frac{1}{2} e_p^\top e_p + 1 - e_\varphi^2 + \frac{1}{2} e_{v_f}^\top \widetilde{M}(x) e_{v_f} + \frac{1}{2} e_\theta^\top \Gamma^{-1} e_\theta + \frac{1}{2\gamma_o} e_\theta^\top e_\theta + \frac{1}{2} e_d^\top B^{-1} e_d + \frac{1}{2\beta_o} e_d^\top e_d,$$

and the design (29a), we conclude by proceeding with a similar analysis that $(e_p, \|e_\epsilon\| e_\varphi, e_{v_f}) \rightarrow (0_3, 0, 0_6)$, which implies that the system is asymptotically driven to either the configuration $(e_p, e_{v_f}, e_\varphi, e_\epsilon) = (0_3, 0_6, \pm 1, 0_3)$, which is the desired one, or a configuration $(e_p, e_{v_f}, e_\varphi, e_\epsilon) = (0_3, 0_6, 0, \tilde{e}_\epsilon)$, where $\tilde{e}_\epsilon \in S^2$ is a unit vector. The latter represents a set of invariant undesired equilibrium points. The closed loop dynamics are the following:

$$\frac{\partial}{\partial t} e_\varphi = \frac{1}{2} e_\varphi \|e_\epsilon\|^2 + \frac{1}{2} [0_3^\top, e_\epsilon^\top] e_v, \quad (31a)$$

$$\frac{\partial}{\partial t} (\|e_\epsilon\|^2) = -e_\varphi^2 \|e_\epsilon\|^2 - e_\varphi [0_3^\top, e_\epsilon^\top] e_v. \quad (31b)$$

We can conclude from the term $[0_3^\top, e_\epsilon^\top] e_v$ in (31) that there exist trajectories that can bring the system close to the undesired equilibrium, rendering thus the point $(e_p, e_{v_f}, e_\varphi, e_\epsilon) = (0_3, 0_6, \pm 1, 0_3)$ only locally asymptotically stable. It has been proved that $e_\varphi = \pm 1$ cannot be globally stabilized with a purely continuous controller [53]. Discontinuous control laws have also been proposed (e.g., [54]), whose combination with adaptation techniques constitutes part of our future research

directions. Another possible direction is tracking directly on $SO(3)$ (see e.g., [55]).

Remark 3 (Robustness (adaptive controller)). Notice also that the control protocol compensates the uncertain dynamic parameters and external disturbances through the adaptation laws (28), although the errors (22), (23) do not converge to zero, but remain bounded. Finally, the control gains k_p, k_ζ, K_v can be tuned appropriately so that the proposed control inputs do not reach motor saturations in real scenarios.

B. Prescribed Performance Control

In this section, we adopt the concepts and techniques of prescribed performance control, recently proposed in [45], in order to achieve predefined transient and steady state response for the derived error, as well as ensure that $\theta_o(t) \in (-\frac{\pi}{2}, \frac{\pi}{2}), \forall t \in \mathbb{R}_{\geq 0}$. As stated in Section II-C, prescribed performance characterizes the behavior where a signal evolves strictly within a predefined region that is bounded by absolutely decaying functions of time, called performance functions. This signal is represented by the object's pose error

$$e_s := \begin{bmatrix} e_{s_x} \\ e_{s_y} \\ e_{s_z} \\ e_{s_\phi} \\ e_{s_\theta} \\ e_{s_\psi} \end{bmatrix} := x_o - x_d(t) \quad (32)$$

First, we reformulate Assumption 4, which is now required to be less strict, stating that the functions d_o, d_i are bounded in time and continuous in the state variables:

Assumption 5 (Uncertainties/Disturbance bound). •

For each fixed $t \in \mathbb{R}_{\geq 0}$, the functions $(x_o, \dot{x}_o) \rightarrow d_o(x_o, \dot{x}_o, t)$ and $(q_i, \dot{q}_i) \rightarrow d_o(q_i, \dot{q}_i, t)$ are continuous, $\forall i \in \mathcal{N}$.

- There exist positive, finite unknown constants $\underline{d}_o, \underline{d}_i$ such that, for each fixed $(x_o, \dot{x}_o) \in \mathbb{M} \times \mathbb{R}^6$ and $(q_i, \dot{q}_i) \in \mathbb{R}^{2n_i}$, the functions $t \rightarrow d_o(x_o, \dot{x}_o, t)$ and $t \rightarrow d_i(q_i, \dot{q}_i, t)$ are bounded by \underline{d}_o and \underline{d}_i , respectively, i.e., $\|d_o(x_o, \dot{x}_o, t)\| \leq \underline{d}_o$, and $\|d_i(q_i, \dot{q}_i, t)\| \leq \underline{d}_i, \forall t \in \mathbb{R}_{\geq 0}, i \in \mathcal{N}$.

The mathematical expressions of prescribed performance are given by the following inequalities:

$$-\rho_{s_k}(t) < e_{s_k}(t) < \rho_{s_k}(t), \forall k \in \mathcal{K}, \quad (33)$$

where $\mathcal{K} := \{x, y, z, \phi, \theta, \psi\}$ and $\rho_k : \mathbb{R}_{\geq 0} \rightarrow \mathbb{R}_{>0}$, with

$$\rho_{s_k}(t) := (\rho_{s_k,0} - \rho_{s_k,\infty}) \exp(-l_{s_k} t) + \rho_{s_k,\infty}, \forall k \in \mathcal{K}, \quad (34)$$

are designer-specified, smooth, bounded and decreasing positive functions of time with $l_{s_k}, \rho_{s_k,\infty}, k \in \mathcal{K}$, positive parameters incorporating the desired transient and steady state performance respectively. The terms $\rho_{s_k,\infty}$ can be set arbitrarily small, achieving thus practical convergence of the errors to zero. Next, we propose a state feedback control protocol that does not incorporate any information on the agents' or the object's dynamics or the external disturbances and guarantees (33) for all $t \in \mathbb{R}_{\geq 0}$. Given the errors (32):

Step I-a. Select the corresponding functions ρ_{s_k} as in (34) with

- (i) $\rho_{s_\theta,0} = \rho_{s_\theta}(0) = \theta^*, \rho_{s_k,0} = \rho_{s_k}(0) > |e_{s_k}(0)|, \forall k \in \mathcal{K} \setminus \{\theta\}$,
- (ii) $l_{s_k} \in \mathbb{R}_{>0}, \forall k \in \mathcal{K}$,
- (iii) $\rho_{s_k,\infty} \in (0, \rho_{s_k,0}), \forall k \in \mathcal{K}$,

where θ^* is a positive constant satisfying $\theta^* + \bar{\theta} < \frac{\pi}{2}$ and $\bar{\theta}$ is the desired trajectory bound (see statement of Problem 1).

Step I-b. Introduce the transformed states representing the normalized errors

$$\xi_s := \begin{bmatrix} \xi_{s_x} \\ \vdots \\ \xi_{s_\psi} \end{bmatrix} := [\rho_s(t)]^{-1} e_s, \quad (35)$$

where $\rho_s(t) := \text{diag}\{[\rho_{s_k}(t)]_{k \in \mathcal{K}}\} \in \mathbb{R}^{6 \times 6}$, as well as the transformed state functions ε_s , and signals $r_s : (-1, 1)^6 \rightarrow \mathbb{R}^{6 \times 6}$, with

$$\varepsilon_s := \begin{bmatrix} \varepsilon_{s_x} \\ \vdots \\ \varepsilon_{s_\psi} \end{bmatrix} := \begin{bmatrix} \ln \left(\frac{1 + \xi_{s_x}}{1 - \xi_{s_x}} \right) \\ \vdots \\ \ln \left(\frac{1 + \xi_{s_\psi}}{1 - \xi_{s_\psi}} \right) \end{bmatrix} \quad (36)$$

$$\begin{aligned} r_s(\xi_s) &:= \text{diag}\{[r_{s_k}]_{k \in \mathcal{K}}\} := \text{diag}\left\{ \left[\frac{\partial \varepsilon_{v_k}(\xi_{s_k})}{\partial \xi_{s_k}} \right]_{k \in \mathcal{K}} \right\} \\ &= \text{diag}\left\{ \left[\frac{2}{1 - \xi_{s_k}^2} \right]_{k \in \mathcal{K}} \right\}, \end{aligned} \quad (37)$$

and design the reference velocity vector:

$$v_r := -g_s J_o \left(\eta_d(t) + \rho_{s_\eta}(t) \xi_{s_\eta} \right)^{-1} [\rho_s(t)]^{-1} r_s(\xi_s) \varepsilon_s, \quad (38)$$

where $\rho_{s_\eta}(t) := \text{diag}\{\rho_{s_\phi}(t), \rho_{s_\theta}(t), \rho_{s_\psi}(t)\}$, $\xi_{s_\eta} := [\xi_{s_\phi}, \xi_{s_\theta}, \xi_{s_\psi}]^\top$, and we have further used the relation $\xi_s = [\rho_s(t)]^{-1} (x_o - x_d(t))$ from (32) and (35).

Step II-a. Define the velocity error vector

$$e_v := \begin{bmatrix} e_{v_x} \\ \vdots \\ e_{v_\psi} \end{bmatrix} := v_o - v_r, \quad (39)$$

and select the corresponding positive performance functions $\rho_{v_k} : \mathbb{R}_{\geq 0} \rightarrow \mathbb{R}_{>0}$ with $\rho_{v_k}(t) := (\rho_{v_k,0} - \rho_{v_k,\infty}) \exp(-l_{v_k} t) + \rho_{v_k,\infty}$, such that $\rho_{v_k,0} = \|e_{v_k}(0)\| + \alpha, l_{v_k} > 0$ and $\rho_{v_k,\infty} \in (0, \rho_{v_k,0}), \forall k \in \mathcal{K}$, where α is an arbitrary positive constant.

Step II-b. Define the normalized velocity error

$$\xi_v := \begin{bmatrix} \xi_{v_x} \\ \vdots \\ \xi_{v_\psi} \end{bmatrix} := [\rho_v(t)]^{-1} e_v, \quad (40)$$

where $\rho_v(t) := \text{diag}\{[\rho_{v_k}(t)]_{k \in \mathcal{K}}\}$, as well as the transformed states ε_v and signals $r_v : (-1, 1)^6 \rightarrow \mathbb{R}^{6 \times 6}$, with

$$\varepsilon_v := \begin{bmatrix} \varepsilon_{v_x} \\ \vdots \\ \varepsilon_{v_\psi} \end{bmatrix} := \begin{bmatrix} \ln \left(\frac{1 + \xi_{v_x}}{1 - \xi_{v_x}} \right) \\ \vdots \\ \ln \left(\frac{1 + \xi_{v_\psi}}{1 - \xi_{v_\psi}} \right) \end{bmatrix}$$

$$\begin{aligned} r_v(\xi_v) &:= \text{diag}\{[r_{v_k}]_{k \in \mathcal{K}}\} := \text{diag}\left\{ \left[\frac{\partial \varepsilon_{v_k}(\xi_{v_k})}{\partial \xi_{v_k}} \right]_{k \in \mathcal{K}} \right\} \\ &= \text{diag}\left\{ \left[\frac{2}{1 - \xi_{v_k}^2} \right]_{k \in \mathcal{K}} \right\}, \end{aligned}$$

and design the distributed feedback control protocol for each agent $i \in \mathcal{N}$ as

$$u_i := -g_v J_{M_i}(q) [\rho_v(t)]^{-1} r_v(\xi_v) \varepsilon_v, \quad (41)$$

where g_v is a positive constant gain and J_{M_i} as defined in (27).

The control laws (41) can be written in vector form $u := [u_1^\top, \dots, u_N^\top]^\top$, with:

$$u = -g_v G_M^+(q) [\rho_v(t)]^{-1} r_v(\xi_v) \varepsilon_v. \quad (42)$$

Remark 4 (Decentralized manner and robustness (PPC)). Similarly to (29), notice from (41) that each agent $i \in \mathcal{N}$ can calculate its own control signal, without communicating with the rest of the team, rendering thus the overall control scheme decentralized. The terms $l_k, \rho_{k,0}, \rho_{k,\infty}, \alpha, l_{v_k}$, and $\rho_{v_k,\infty}, k \in \mathcal{K}$ needed for the calculation of the performance functions can be transmitted off-line to the agents. Moreover, the Prescribed Performance Control protocol is also robust to uncertainties of model uncertainties and external disturbances. In particular, note that the control laws do not even require the structure of the terms $\tilde{M}, \tilde{C}, \tilde{g}, \tilde{d}$, but only the positive definiteness of M , as will be observed in the subsequent proof of Theorem 3. It is worth noting that, in the case that one or more agent failed to participate in the task, then the remaining agents would need to appropriately update their control protocols (e.g., update the load distributions terms J_{M_i}) to compensate for the failure.

Remark 5 (Internal forces). Internal force regulation can be also guaranteed by including in the control laws (29a) and (42) a term of the form $(I_{6N} - G_M^+(q)G(q)^\top) \hat{f}_{int,d}$, where $\hat{f}_{int,d} \in \mathbb{R}^{6N}$ is a constant vector representing desired internal forces (e.g. to avoid grasp sliding), that can be transmitted off-line to the agents.

The main results of this subsection are summarized in the following theorem.

Theorem 3. Consider N agents rigidly grasping an object with unknown coupled dynamics (15). Then, under Assumptions 1-3, 5, the distributed control protocol (35)-(41) guarantees that $-\rho_{s_k}(t) < e_{s_k}(t) < \rho_{s_k}(t), \forall k \in \mathcal{K}, t \in \mathbb{R}_{\geq 0}$ from all the initial conditions satisfying $|\theta(0) - \theta_d(0)| < \theta^*$ (where θ^* was used in Step I-a (i)), with all closed loop signals being bounded.

Proof: Note first from (32), (35), (39), and (40), that the states x_o, v_o can be expressed as

$$x_o = x_d(t) + \rho_s(t)\xi_s, \quad (43a)$$

$$v_o = \rho_v(t)\xi_v + v_r, \quad (43b)$$

which was used in (38) and will be also used in the sequel.

Consider the combined state $\sigma = [q, \xi_s, \xi_v] \in \mathbb{R}^{n+12}$. From the differential kinematics $v_i = J_i(q_i)\dot{q}_i$, Assumption 3, as well as (10), (39), (40), and noting that v_r in (38) is a function of ξ_s and t , we can derive

$$\begin{aligned} \dot{q} &= \tilde{J}(q)v = \tilde{J}(q)G(q)v_o \\ &= \tilde{J}(q)G(q)\left(\rho_v(t)\xi_v + v_r(\xi_s, t)\right) \\ &=: f_{cl,q}(\sigma, t), \end{aligned} \quad (44)$$

where $\tilde{J}(q) := \text{diag}\{J_i(q_i)^\top(J_i(q_i)J_i(q_i)^\top)^{-1}\}_{i \in \mathcal{N}} \in \mathbb{R}^{6N \times n}$. Next, we obtain from (35):

$$\begin{aligned} \dot{\xi}_s &= [\rho(t)]^{-1}\left(\dot{e} - \dot{\rho}_s(t)\xi_s\right), \\ &= [\rho(t)]^{-1}\left(\dot{x}_o - \dot{x}_d(t) - \dot{\rho}_s(t)\xi_s\right), \end{aligned}$$

which, after employing (7a), (32), (38), as well as (43), becomes

$$\begin{aligned} \dot{\xi}_s &= [\rho(t)]^{-1}\left[J_o\left(\eta_d(t) + \rho_{s_\eta}(t)\xi_{s_\eta}\right)\rho_v(t)\xi_v - \dot{\rho}_s(t)\xi_s \right. \\ &\quad \left. - g_s[\rho(t)]^{-1}r_s(\xi_s)\varepsilon_s - \dot{x}_d(t)\right] =: f_{cl,s}(\sigma, t). \end{aligned} \quad (45)$$

By differentiating v_r , and using (43), (35), (37), we obtain

$$\begin{aligned} \dot{v}_r &= -g_s J_o\left(\eta_d(t) + \rho_{s_\eta}(t)\xi_s\right)^{-1}\left[[\rho_s(t)]^{-1}\dot{r}_s(\xi_s)\varepsilon_s \right. \\ &\quad \left. + [\rho_s(t)]^{-1}[r_s(\xi_s)]^2 f_{cl,s}(\sigma, t) - [\rho_s(t)]^{-2}\dot{\rho}_s(t)r_s(\xi_s)\varepsilon_s\right] \\ &\quad - g_s \frac{\partial}{\partial t}\left[J_o(\eta_o)^{-1}\right][\rho_s(t)]^{-1}r_s(\xi_s)\varepsilon_s(\xi_s), \end{aligned} \quad (46)$$

where

$$\begin{aligned} \dot{r}_s(\xi_s) &= \text{diag}\left\{\left[\frac{2\xi_{s_k}}{(1-\xi_{s_k})^2}\right]_{k \in \mathcal{K}}\right\} \sum_{k \in \mathcal{K}} \bar{E}_k \dot{\xi}_s \bar{e}_k \\ &= \text{diag}\left\{\left[\frac{2\xi_{s_k}}{(1-\xi_{s_k})^2}\right]_{k \in \mathcal{K}}\right\} \sum_{k \in \mathcal{K}} \bar{E}_k f_{cl,s}(\sigma, t) \bar{e}_k, \end{aligned}$$

with $\bar{E}_k \in \mathbb{R}^{6 \times 6}$ being the matrix with 1 in the position (k, k) and zeros everywhere else, and $\bar{e}_k \in \mathbb{R}^6$ being the vector with 1 in the position k and zeros everywhere else. Note from (46), (43), and the fact that $\dot{x}_o = J_o(\eta_d(t) + \rho_{s_\eta}(t)\xi_{s_\eta})v_o$ that \dot{v}_r can be expressed as a function of σ and t .

Moreover, from (39) and (40) one obtains:

$$\begin{aligned} \dot{\xi}_v &= [\rho_v(t)]^{-1}\left(\dot{e}_v - \dot{\rho}_v(t)\xi_v\right), \\ &= [\rho_v(t)]^{-1}\left(\dot{v}_o - \dot{v}_r(\sigma, t) - \dot{\rho}_v(t)\xi_v\right), \end{aligned}$$

which, after employing (15), (42), and the fact that $[G(q)]^\top G_M^+ = I_6$, becomes

$$\begin{aligned} \dot{\xi}_v &= [\rho_v(t)]^{-1}\left(-\dot{\rho}_v(t)\xi_v - \tilde{M}(x(\sigma, t))\left[\tilde{C}(x(\sigma, t))[\rho_v(t)\xi_v + \right. \right. \\ &\quad \left. \left. v_r(\xi_s, t)\right] + \tilde{g}(x(\sigma, t)) + \tilde{d}(x(\sigma, t), t) - \right. \\ &\quad \left. g_v[\rho_v(t)]^{-1}r_v(\xi_v)\varepsilon_v(\xi_v)\right] - \dot{v}_r(\sigma, t) =: f_{cl,v}(\sigma, t) \end{aligned} \quad (47)$$

and where, by using (43) and (44), we have written x (that was first defined in (15)) as a function of σ and t , i.e.,

$$x(\sigma, t) = \begin{bmatrix} q \\ \dot{q} \\ x_o \\ \dot{x}_o \end{bmatrix} = \begin{bmatrix} q \\ f_{cl,q}(\sigma, t) \\ x_d(t) + \rho_s(t)\xi_s \\ J_o\left(\eta_d(t) + \rho_{s_\eta}(t)\xi_{s_\eta}\right)[\rho_v(t)\xi_v + v_r(\xi_s, t)] \end{bmatrix}.$$

Hence, we can write (44)-(47) in compact form

$$\dot{\sigma} = f_{cl}(\sigma, t) := \begin{bmatrix} f_{cl,q}(\sigma, t) \\ f_{cl,s}(\sigma, t) \\ f_{cl,v}(\sigma, t) \end{bmatrix}.$$

Consider now the open and nonempty set $\Omega := \mathbb{R}^n \times (-1, 1)^{12}$. The choice of the parameters $\rho_{s_k,0}$ and $\rho_{v_k,0}$, $k \in \mathcal{K}$ in **Step I-a** and **Step II-a**, respectively, along with the fact that the initial conditions satisfy $|\theta_o(0) - \theta_d(0)| < \theta^*$ imply that $|e_{s_k}(0)| < \rho_{s_k}(0)$, $|e_{v_k}(0)| < \rho_{v_k}(0)$, $\forall k \in \mathcal{K}$ and hence $[\xi_s(0)^\top, \xi_v(0)^\top]^\top \in (-1, 1)^{12}$. Moreover, it can be verified that $f_{cl} : \Omega \times \mathbb{R}_{\geq 0} \rightarrow \mathbb{R}^{n+12}$ is locally Lipschitz in σ over the set Ω and is continuous in t , which makes it also locally integrable in t for each fixed $\sigma \in \Omega$. Therefore, the hypotheses of Theorem 1 stated in Subsection II-D hold and the existence of a maximal solution $\sigma : [0, \tau_{\max}) \rightarrow \Omega$, for $\tau_{\max} > 0$, is ensured. We thus conclude that

$$\xi_{s_k}(t) = \frac{e_{s_k}(t)}{\rho_{s_k}(t)} \in (-1, 1), \quad (48a)$$

$$\xi_{v_k}(t) = \frac{e_{v_k}(t)}{\rho_{v_k}(t)} \in (-1, 1), \quad (48b)$$

$\forall k \in \mathcal{K}, t \in [0, \tau_{\max})$, which also implies that $\|\xi_s(t)\| \leq \sqrt{6}$, and $\|\xi_v(t)\| \leq \sqrt{6}, \forall t \in [0, \tau_{\max})$. Next, we need to show the boundedness of all closed loop signals as well as that $\tau_{\max} = \infty$. Note first from (48), that $|\theta_o(t) - \theta_d(t)| < \rho_\theta(t) \leq \rho_\theta(0) = \theta^*$, which, since $\theta_d(t) \in [-\bar{\theta}, \bar{\theta}], \forall t \in \mathbb{R}_{\geq 0}$, implies that $|\theta_o(t)| \leq \bar{\theta} := \bar{\theta} + \theta^* < \frac{\pi}{2}, \forall t \in [0, \tau_{\max})$. Therefore, by employing (8), one obtains

$$\|J_o(\eta_o(t))\| \leq \bar{J}_o := \sqrt{\frac{|\sin(\bar{\theta})| + 1}{1 - \sin^2(\bar{\theta})}} < \infty, \quad \forall t \in [0, \tau_{\max}). \quad (49)$$

Consider now the positive definite and radially unbounded function $V_s : \mathbb{R}^6 \rightarrow \mathbb{R}_{\geq 0}$, with $V_s(\varepsilon_s) = \frac{1}{2}\|\varepsilon_s\|^2$, and its derivative along the solutions of the closed loop system, which, in view of (45), yields

$$\begin{aligned} \dot{V}_s(\varepsilon_s) &= -g_s\|\rho_s(t)^{-1}r_s(\xi_s)\varepsilon_s\|^2 + \\ &\quad [\varepsilon_s(\xi_s)]^\top r_s(\xi_s)\rho_s(t)^{-1}\left(J_o(\eta_d(t) + \rho_{s_\eta}(t)\xi_{s_\eta})\rho_v(t)\xi_v \right. \\ &\quad \left. - \dot{x}_d(t) - \dot{\rho}_s(t)\xi_s\right) \\ &\leq g_s\|\rho(t)^{-1}r_s(\xi_s)\varepsilon_s\|^2 + \\ &\quad \|\rho_s(t)^{-1}r_s(\xi_s)\varepsilon_s\|\left(\|J_o(\eta_d(t) + \rho_{s_\eta}(t)\xi_{s_\eta})\rho_v(t)\xi_v\| \right. \\ &\quad \left. + \|\dot{x}_d(t)\| + \|\dot{\rho}_s(t)\xi_s\|\right). \end{aligned}$$

In view of (49), (48), and the structure of $\rho_{s_k}, \rho_{v_k}, k \in \mathcal{K}$, as well as the fact that $v_o(0) = 0$ and the boundedness of $\dot{x}_d(t)$, the last inequality becomes

$$\begin{aligned} \dot{V}_s(\varepsilon_s) &\leq -g_s \|\rho_s(t)^{-1} r_s(\xi_s) \varepsilon_s\|^2 + \\ &\quad \|\rho_s(t)^{-1} r_s(\xi_s) \varepsilon_s\| \bar{B}_s, \end{aligned}$$

$\forall t \in [0, \tau_{\max})$, where

$$\bar{B}_s := \sqrt{6} \bar{J}_o (\|v_r(0)\| + \alpha) + \bar{x}_d + \sqrt{6} \max_{k \in \mathcal{K}} \{l_k(\rho_{s_k,0} - \rho_{s_k,\infty})\},$$

is a positive constant independent of τ_{\max} , \bar{x}_d is the bound of $\dot{x}_d(t)$. Therefore, $\dot{V}_s(\varepsilon_s)$ is negative when $\|\rho_s(t)^{-1} r_s(\xi_s) \varepsilon_s\| > \frac{\bar{B}_s}{g_s}$, which, by employing (37), the decreasing property of $\rho_{s_k}(t), k \in \mathcal{K}$ as well as (48a), is satisfied when $\|\varepsilon_s\| > \frac{\max_{k \in \mathcal{K}} \{\rho_{s_k,0}\} \bar{B}_s}{2g_s}$. Hence, we conclude that

$$\|\varepsilon_s(t)\| \leq \bar{\varepsilon}_s := \max \left\{ \|\varepsilon_s(0)\|, \frac{\max_{k \in \mathcal{K}} \{\rho_{s_k,0}\} \bar{B}_s}{2g_s} \right\}, \quad (50)$$

$\forall t \in [0, \tau_{\max})$. Furthermore, since $|\varepsilon_{s_k}| \leq \|\varepsilon_s\|, \forall k \in \mathcal{K}$, taking the inverse logarithm function from (36), we obtain

$$-1 < \frac{\exp(-\bar{\varepsilon}_s) - 1}{\exp(-\bar{\varepsilon}_s) + 1} =: -\bar{\xi}_s \leq \xi_{s_k}(t) \leq \bar{\xi}_s := \frac{\exp(\bar{\varepsilon}_s) - 1}{\exp(\bar{\varepsilon}_s) + 1} < 1, \quad (51)$$

$\forall t \in [0, \tau_{\max})$. Hence, recalling (37), one obtains

$$\|r_s(\xi_s(t))\| \leq \bar{r}_s := \frac{2}{1 - \bar{\xi}_s^2} = \frac{(\exp(\bar{\varepsilon}_s) + 1)^2}{2 \exp(\bar{\varepsilon}_s)},$$

$\forall t \in [0, \tau_{\max})$. Therefore, we obtain from (38) the boundedness of v_r with

$$\|v_r(t)\| \leq \bar{v}_r := g_s \sqrt{2} \frac{\bar{\varepsilon}_s (\exp(\bar{\varepsilon}_s) + 1)^2}{2 \min_{k \in \mathcal{K}} \{\rho_{s_k,\infty}\} \exp(\bar{\varepsilon}_s)}, \quad (52)$$

$\forall t \in [0, \tau_{\max})$. Since $v_o = v_r + \rho_v(t) \xi_v$, we also conclude that

$$\|v_o(t)\| \leq \bar{v}_o := g_s \sqrt{2} \frac{\bar{\varepsilon}_s (\exp(\bar{\varepsilon}_s) + 1)^2}{2 \min_{k \in \mathcal{K}} \{\rho_{k,\infty}\} \exp(\bar{\varepsilon}_s)} + \sqrt{6} \max_{k \in \mathcal{K}} \{\rho_{v_k,0}\}, \quad (53)$$

$\forall t \in [0, \tau_{\max})$, which, through (10) and (13), leads to

$$\|v_i(t)\| \leq \bar{v}_i := (\|p_{o/E_i}^E\| + 1) \bar{v}_o, \forall i \in \mathcal{N}, t \in [0, \tau_{\max}). \quad (54)$$

In a similar vein, we can also derive a bound for the derivative of the reference velocity (46), $\|\dot{v}_r(t)\| \leq \bar{v}_r, \forall t \in [0, \tau_{\max})$, which is not written explicitly for presentation clarity. From (51), (7a), and (32) we also conclude that $\|x_o(t)\| \leq \bar{x}_o := \bar{x}_d + \sqrt{6} \bar{\xi}_s \max_{k \in \mathcal{K}} \{\rho_{s_k,0}\}, t \in [0, \tau_{\max})$, as well as $\|\dot{x}_o(t)\| \leq \bar{J}_o \bar{v}_o$.

Applying the aforementioned line of proof, we consider the positive definite and radially unbounded function $V_v : \mathbb{R}^6 \rightarrow \mathbb{R}_{\geq 0}$, with $V_v(\varepsilon_v) = \frac{1}{2} \|\varepsilon_v\|^2$, and its derivative along the solutions of the closed loop system, which, in view of (47), yields

$$\begin{aligned} \dot{V}_v(\varepsilon_v) &= -g_v \varepsilon_v^\top r_v(\xi_v) \rho_v(t)^{-1} \widetilde{M}(x) \rho_v(t)^{-1} r_v(\xi_v) \varepsilon_v \\ &\quad + \varepsilon_v^\top r_v(\xi_v) \rho_v(t)^{-1} \left(-\dot{\rho}_v(t) \xi_v - \widetilde{M}(x) \left[\widetilde{C}(x) [\rho_v(t) \xi_v + \right. \right. \\ &\quad \left. \left. v_r \right] + \widetilde{g}(x) + \widetilde{d}(x, t) \right] - \dot{v}_r \right), \end{aligned} \quad (55)$$

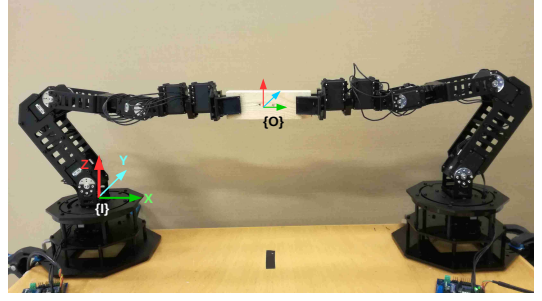


Fig. 2: Two WidowX Robot Arms rigidly grasping an object.

By using (9) and the fact that the rotation matrix $R_{E_i}(q_i)$ is an orthogonal matrix, we obtain $\|x_{E_i}(t)\| := \|p_{E_i}^\top(q_i(t), \eta_{E_i}^\top(q_i(t)))^\top\| \leq \|x_o(t)\| + \|[(p_{E_i/o}^E)^\top, \eta_{E_i/o}^\top]^\top\|$ and hence, in view of the inverse kinematics of the agents [43], we conclude the boundedness of $q(t)$ as

$$\|q(t)\| \leq \bar{q}, \forall t \in [0, \tau_{\max}), \quad (56)$$

where \bar{q} is a positive constant. From Assumption 3 and the forward differential agent kinematics, we can also conclude that there exists a positive constant \bar{J} such that $\|\dot{q}(t)\| \leq \bar{J} \|v\| \leq \bar{J} \sum_{i \in \mathcal{N}} \bar{v}_i, \forall t \in [0, \tau_{\max})$, where \bar{v}_i was defined in (54). Therefore, we conclude that

$$\|x(t)\| \leq \bar{x} := \bar{q} + \bar{J} \sum_{i \in \mathcal{N}} \bar{v}_i + \bar{x}_o + \bar{J}_o \bar{v}_o, \quad (57)$$

$\forall t \in [0, \tau_{\max})$.

Invoking Assumption 5 and the boundedness of the states $q_i(t), \dot{q}_i(t), x_o(t), \dot{x}_o(t), \forall t \in [0, \tau_{\max})$, we conclude the boundedness of $d_o(x_o(t), \dot{x}_o(t), t)$ and $d_i(q_i(t), \dot{q}_i(t), t), \forall t \in [0, \tau_{\max})$, by positive and finite constants \underline{d}'_o and \underline{d}'_i , respectively, $\forall i \in \mathcal{N}$. Hence, from expressions (13) and (16d), we obtain $\|\widetilde{d}(x(t))\| \leq \underline{d} := \underline{d}'_o + \sum_{i \in \mathcal{N}} \{\|p_{o/E_i}^E\| + 1\} \underline{d}'_i$.

In addition, since the terms $\widetilde{C}(x), \widetilde{g}(x)$ are continuous, we conclude from (57) that there exist positive constants \bar{c}, \bar{g} , independent of τ_{\max} (since \bar{x} is also independent of τ_{\max}), such that $\|\widetilde{C}(x(t))\| \leq \bar{c}, \|\widetilde{g}(x(t))\| \leq \bar{g}, \forall t \in [0, \tau_{\max})$.

Thus, by combining the aforementioned results along with the boundedness of v_r , (48), (52), (57) as well as (17), we obtain from (55)

$$\dot{V}_v(\varepsilon_v) \leq -g_v \underline{m} \|\rho_v(t)^{-1} r_v(\xi_v) \varepsilon_v\|^2 + \|\rho_v(t)^{-1} r_v(\xi_v) \varepsilon_v\| \bar{B}_v,$$

$\forall t \in [0, \tau_{\max})$, where

$$\begin{aligned} \bar{B}_v &:= \sqrt{6} \max_{k \in \mathcal{K}} \{l_{v_k}(\rho_{v_k,0} - \rho_{v_k,\infty})\} + \bar{v}_r + \underline{m} (\bar{g} + \underline{d} + \\ &\quad \bar{c}(\bar{v}_r + \sqrt{6}(\|v_r(0)\| + \alpha))). \end{aligned} \quad (58)$$

By proceeding similarly as with $\dot{V}_s(\varepsilon_s)$, we conclude that

$$\|\varepsilon_v(t)\| \leq \bar{\varepsilon}_v := \max \left\{ \|\varepsilon_v(0)\|, \frac{\max_{k \in \mathcal{K}} \{\rho_{v_k,0}\} \bar{B}_v}{2g_v \underline{m}} \right\}, \quad (59)$$

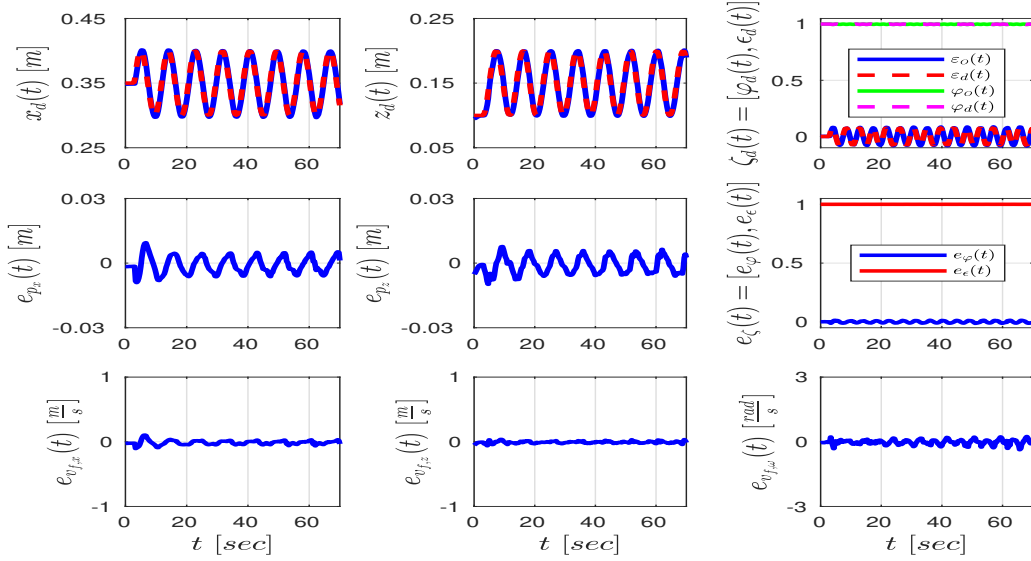


Fig. 3: Simulations results for the controller of subsection IV-A, for $t \in [0, 70]$ [sec]. Top: The desired (with blue) and actual (with red) object trajectory in x - and z -axis as well as the quaternion desired and actual object trajectory. Middle: The position and quaternion errors $e_p(t)$, $e_c(t)$, respectively. Bottom: The velocity errors $e_{v_f}(t)$.

$\forall t \in [0, \tau_{\max})$, from which we obtain

$$-1 < \frac{\exp(-\bar{\varepsilon}_v) - 1}{\exp(-\bar{\varepsilon}_v) + 1} =: -\bar{\xi}_v \leq \xi_{v_k}(t) \leq \bar{\xi}_v := \frac{\exp(\bar{\varepsilon}_v) - 1}{\exp(\bar{\varepsilon}_v) + 1} < 1, \quad (60)$$

as well as

$$\|r_v(\xi_v(t))\| \leq \bar{r}_v := \frac{2}{1 - \bar{\xi}_v^2} = \frac{(\exp(\bar{\varepsilon}_v) + 1)^2}{2 \exp(\bar{\varepsilon}_v)},$$

$\forall t \in [0, \tau_{\max})$. Moreover, it can be shown, from the fact that $p_{O/E_i} = R_O(q_i)p_{O/E_i}^O$, $\forall i \in \mathcal{N}$, that the norm $\|J_{M_i}(q)\|$, as defined in (27), is independent of q . Hence, we can also conclude the boundedness of the control inputs (41)

$$\|u_i(t)\| \leq \bar{u}_i := g_v \|J_{M_i}(q)\| \max_{k \in \mathcal{K}} \left\{ \frac{1}{\rho_{v_k, \infty}} \right\} \bar{r}_v \bar{\varepsilon}_v, \quad \forall t \in [0, \tau_{\max}). \quad (61)$$

What remains to be shown is that $\tau_{\max} = \infty$. To this end, note from (56), (51), (60), that the solution $\sigma(t)$ remains in a compact subset of $\Omega = \mathbb{R}^n \times (-1, 1)^{12}$, i.e.,

$$\sigma(t) \in \Omega' := [-\bar{q}, \bar{q}] \times [-\bar{\xi}_s, \bar{\xi}_s]^6 \times [-\bar{\xi}_v, \bar{\xi}_v]^6,$$

$\forall t \in [0, \tau_{\max})$. Hence, assuming $\tau_{\max} < \infty$ and since $\Omega' \subset \Omega$, Proposition 1 in Subsection II-D dictates the existence of a time instant $t' \in [0, \tau_{\max})$ such that $\sigma(t') \notin \Omega'$, which is a contradiction. Therefore, $\tau_{\max} = \infty$. Thus, all closed loop signals remain bounded and moreover $\sigma(t) \in \Omega' \subset \Omega, \forall t \in \mathbb{R}_{\geq 0}$. Finally, by multiplying (51) by $\rho_k(t), k \in \mathcal{K}$, we obtain

$$-\rho_{s_k}(t) < -\bar{\xi}_s \rho_{s_k}(t) \leq e_{s_k}(t) \leq \bar{\xi}_s \rho_{s_k}(t) < \rho_{s_k}(t), \quad (62)$$

$\forall t \in \mathbb{R}_{\geq 0}$, which leads to the conclusion of the proof. \blacksquare

Remark 6 (Prescribed Performance). From the aforementioned proof it can be deduced that the Prescribed Performance Control scheme achieves its goal without resorting to the need of rendering the ultimate bounds $\bar{\varepsilon}_s, \bar{\varepsilon}_v$ of the

modulated pose and velocity errors $\varepsilon_s(t), \varepsilon_v(t)$ arbitrarily small by adopting extreme values of the control gains g_s and g_v (see (50) and (59)). More specifically, notice that (51) and (60) hold no matter how large the finite bounds $\bar{\varepsilon}_s, \bar{\varepsilon}_v$ are. In the same spirit, large uncertainties involved in the coupled model (15) can be compensated, as they affect only the size of ε_v through \bar{B}_v (see (58)), but leave unaltered the achieved stability properties. Hence, the actual performance given in (62), which is solely determined by the designed-specified performance functions $\rho_{s_k}(t), \rho_{v_k}(t), k \in \mathcal{K}$, becomes isolated against model uncertainties, thus extending greatly the robustness of the proposed control scheme.

Remark 7 (Control Input Bounds). The aforementioned analysis of the Prescribed Performance Control methodology reveals the derivation of implicit bounds for the velocity v_i and control input u_i of each agent. More specifically, notice that (54) and (53) provide a bound for the agents' velocity, $\|v_i(t)\| \leq \bar{v}_i$. Therefore, given a bound for the agents' velocity $\bar{v}_{i,b}$ (derived from bounds on the joint velocities \bar{q}_i), $i \in \mathcal{N}$, the desired trajectory velocity bound \bar{x}_d , as well as the initial velocity error $v_\tau(0)$ (which is proportional to $\varepsilon_s(0)$), we can tune appropriately the control gain g_s as well as the parameters $\rho_{s_k,0}, \rho_{v_k,0}, \rho_{s_k,\infty}, \rho_{v_k,\infty}, l_{s_k}, l_{v_k}$, and α , to achieve $\bar{v}_i \leq \bar{v}_{i,b}, \forall i \in \mathcal{N}$. In the same spirit, (61) provides a bound \bar{u}_i for the control inputs of the agents. Hence, given bounds for the agents' inputs $\bar{u}_{i,b}$ (derived from bounds on the joint torques τ_i), $i \in \mathcal{N}$, if the upper bound term \bar{B}_v is known, we can further tune the control gain g_v as well as the performance function parameters to achieve $\bar{u} \leq \bar{u}_{i,b}$. Explicit closed-loop expressions for the choice of these gains and parameters are beyond the scope of this paper and consist part of future work. It is also worth noting that the selection of the control gains g_s, g_v affects the evolution of the errors e, e_v inside the corresponding performance envelope.

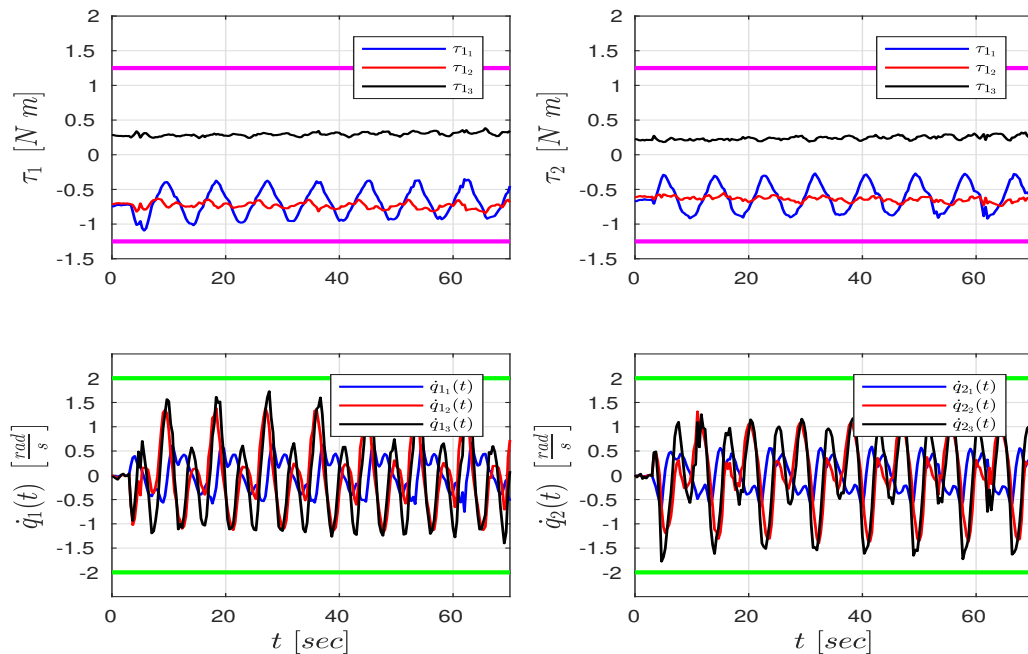


Fig. 4: The agent joint torques and velocities of the simulation of the controller in subsection IV-A, for $t \in [0, 70]$ [sec], with their respective limits (purple and green lines, respectively). Top: The joint torques of agent 1 (left) and agent 2 (right). Bottom: The joint velocities of agent 1 (left) and agent 2 (right).

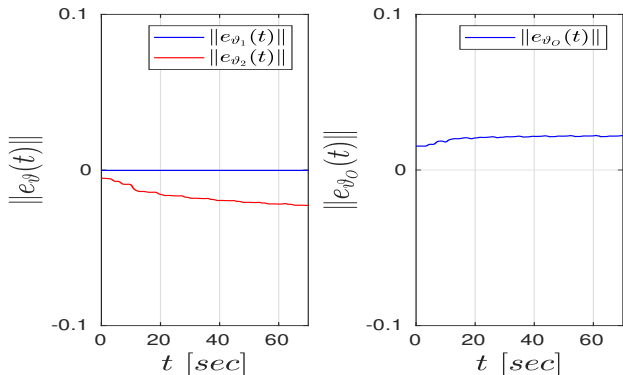


Fig. 5: The norms of the adaptation signals $e_{\vartheta_i}(t), \forall i \in \{1, 2\}$ (left) and $e_{\vartheta_o}(t)$ (right), $\forall t \in [0, 70]$ [sec] of the simulation of the controller in subsection IV-A.

V. SIMULATION AND EXPERIMENTAL RESULTS

In this section, we provide simulation and experimental results for the two developed control schemes. Firstly, in subsection V-A we present results from computer simulations using the realistic environment of V-REP [56] as well as experimental results using the adaptive control protocol developed in Section IV-A. Then, in subsection V-B, we provide simulation and experimental results using the Prescribed Performance Control algorithm developed in Section IV-B.

The tested scenario consists of two WidowX Robot Arms [57] rigidly grasping a wooden cuboid object (see Fig. 2) that has to track a planar time trajectory $p_d(t) = [x_d(t), 0, z_d(t)]^T, \eta_d(t) = [0, \theta_d(t), 0]^T$. For that purpose, we employ the three rotational -with respect to the y axis - joints of the arms. The lower joint consists of a MX-64

Dynamixel Actuator, whereas each of the two upper joints consists of a MX-28 Dynamixel Actuator from the MX Series [58]. Both actuators provide feedback of the joint angle and rate $q_i, \dot{q}_i, \forall i \in \{1, 2\}$. The micro-controller used for the actuators of each arm is the ArbotiX-M Robocontroller [59], which is serially connected to an i-7 desktop computer with 4 cores and 16GB RAM. All the computations for the real-time experiments are performed at a frequency of 120 [Hz] and for the V-REP simulations at 60 [Hz]. Finally, we consider that the MX-64 motor can exert a maximum torque of 3 [Nm], and the MX-28 motors can exert a maximum torque of 1.25 [Nm], values that are slightly more conservative than the actual limits. In the same vein, we also assume a velocity bound of 0.5 [rad/s] for the experiments and 2 [rad/s] for the V-REP simulations. In all cases, we set the load distribution with $m_1^* = m_2^* = 1$, and $J_1^* = 0.75I_3, J_2^* = 0.25I_3$, in order to demonstrate a potential difference in the power capabilities of the agents. A video illustrating the simulation and experimental results accompanies the specific paper.

A. Adaptive Control with Quaternion Feedback

In this subsection, we present simulation and experimental results for the control protocol developed in Section IV-A.

1) *Simulation Results:* The desired trajectory for the V-REP simulations is set to $x_d(t) = 0.35 + 0.05 \sin\left(\frac{2\pi t}{15}\right)$ [m], $z_d(t) = 0.15 - 0.05 \cos\left(\frac{2\pi t}{15}\right)$ [m], which defines a circle in the x - z plane of center (0.35, 0.15) [m] and radius 0.05 [m], and $\theta_d(t) = \frac{\pi}{20} \sin\left(\frac{5\pi t}{15}\right)$ [rad], which is translated to the desired 2D quaternion trajectory $\zeta_d(t) = \left[\cos\left(\frac{\theta_d(t)}{2}\right), 0, 0, \sin\left(\frac{\theta_d(t)}{2}\right) \right]^T$. The simulation results are depicted in Figs. 3-5 for $t \in [0, 70]$ [sec]; Fig. 3 pictures the

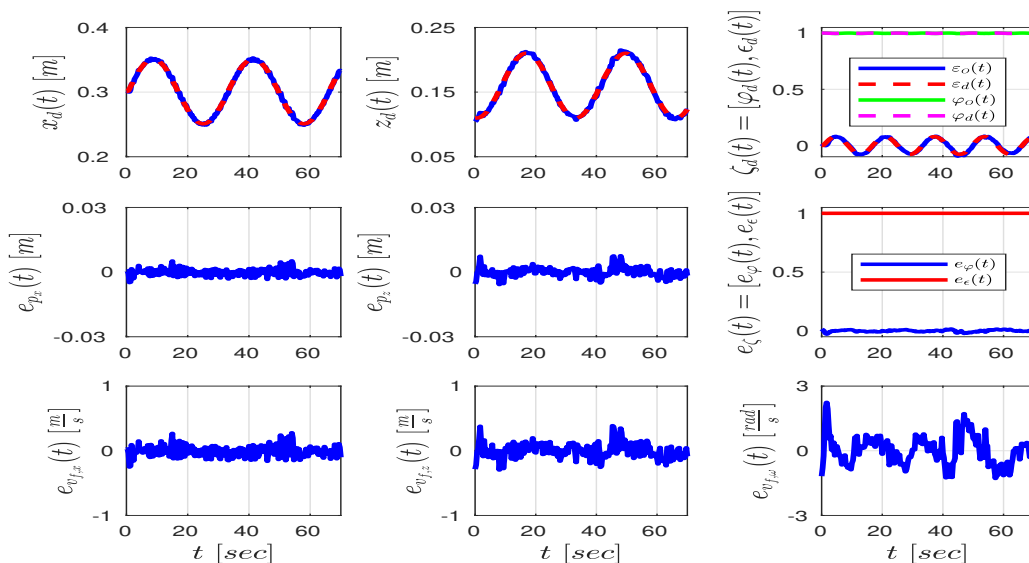


Fig. 6: Experimental results for the controller of subsection IV-A, for $t \in [0, 70]$ [sec]. Top: The desired (with blue) and actual (with red) object trajectory in x - and z -axis as well as the quaternion desired and actual object trajectory. Middle: The position and quaternion errors $e_p(t)$, $e_{\zeta}(t)$, respectively. Bottom: The velocity errors $e_{v_f}(t)$.

desired and actual trajectory of the object's center of mass (top), the pose errors $e_p(t)$, $e_{\zeta}(t)$ (middle), as well as the velocity error $e_{v_f}(t)$ (bottom). We can verify from the figure that the desired trajectory is tracked almost perfectly, with negligible oscillations. The control inputs as well as the agent velocities with their respective limits are illustrated in Fig. 4. By appropriately tuning the control gains, which were set as $k_p = 15$, $k_{\zeta} = 30$, $K_{v_1} = K_{v_2} = \text{diag}\{5, 2, 0.1\}$, we achieved confinement of the signals in the domain formed by the limits. Note also the difference due to the different load sharing coefficients. Finally, Fig. 3 depicts the norms of the adaptation signals $e_{\vartheta_i}(t)$ and $e_{\vartheta_o}(t)$, $\forall i \in \{1, 2\}$, which, as proven in the theoretical analysis, remain bounded. The functions $\delta_o(x_o, \dot{x}_o, t)$, $\delta_i(q_i, \dot{q}_i, t)$ were taken as $0_{6 \times \mu_o}$ and $0_{6 \times \mu_i}$, respectively, and hence, the adaptation controller (28c), (28d) were not employed. Loosely speaking, the disturbances $d_o(x_o, \dot{x}_o, t)$, $d_i(q_i, \dot{q}_i, t)$ were not taken into account in our model, without, however, degrading the performance of the proposed scheme.

2) *Experimental Results:* The desired trajectory for the experimental results of the controller developed in Section IV-A was set to $x_d(t) = 0.3 + 0.05 \sin\left(\frac{2\pi t}{35}\right)$ [m], $z_d(t) = 0.15 - 0.05 \cos\left(\frac{2\pi t}{35}\right)$ [m], which defines a similar circle with the simulations section, and $\theta_d(t) = \frac{\pi}{20} \sin\left(\frac{5\pi t}{35}\right)$ [rad], which is translated to the corresponding desired 2D quaternion trajectory $\zeta_d(t) = \left[\cos\left(\frac{\theta_d(t)}{2}\right), 0, 0, \sin\left(\frac{\theta_d(t)}{2}\right)\right]^{\top}$. The control gains here were chosen as $k_p = 50$, $k_{\zeta} = 80$, $K_{v_1} = K_{v_2} = \text{diag}\{3.5, 0.5, 0.5\}$. The disturbances $d_o(x_o, \dot{x}_o, t)$, $d_i(q_i, \dot{q}_i, t)$ were also not taken into account in this case, by setting the functions $\delta_o(x_o, \dot{x}_o, t)$, $\delta_i(q_i, \dot{q}_i, t)$ to $0_{6 \times \mu_o}$ and $0_{6 \times \mu_i}$, respectively. The simulation results are depicted in Figs. 6-8 for $t \in [0, 70]$ [sec]; Fig. 6 pictures the desired and actual trajectory of the object's center of mass (top), the pose errors $e_p(t)$, $e_{\zeta}(t)$ (middle), as well as the

velocity error $e_{v_f}(t)$ (bottom). We can verify from the figure that the desired trajectory is tracked also for the experimental case, with oscillations in the velocity errors, which can be attributed to model uncertainties, sensor noise, or the unmodeled external disturbances, that have a larger effect in this (experimental) scenario. The control inputs as well as the agent velocities with their respective limits are illustrated in Fig. 7, which are confined in their respective limits. Finally, Fig. 6 depicts the norms of the adaptation signals $e_{\vartheta_i}(t)$ and $e_{\vartheta_o}(t)$, $\forall i \in \{1, 2\}$, which are bounded in this case as well.

B. Prescribed Performance Control

In this subsection, we present simulation and experimental results for the control protocol developed in Section IV-B.

1) *Simulation Results:* The desired trajectory in this subsection was chosen the same as in subsection V-A1, i.e., $x_d(t) = 0.35 + 0.05 \sin\left(\frac{2\pi t}{15}\right)$ [m], $z_d(t) = 0.15 - 0.05 \cos\left(\frac{2\pi t}{15}\right)$ [m], and $\theta_d(t) = \frac{\pi}{20} \sin\left(\frac{5\pi t}{15}\right)$ [rad]. The prescribed performance functions are chosen as: $\rho_{s_x}(t) = \rho_{s_z}(t) = 0.03 \exp(-0.5t) + 0.01$ [m], $\rho_{s_{\theta}}(t) = 0.45 \exp(-0.5t) + 0.05$ [rad], $\rho_{v_x}(t) = 3 \exp(-0.5t) + 4$ [m/s], $\rho_{v_z}(t) = 5 \exp(-0.5t) + 5$ [m/s], and $\rho_{v_{\theta}}(t) = 5 \exp(-0.5t) + 5$ [rad/s]. The simulation results are depicted in Figs. 9 and 10; Fig. 9 shows the desired and actual trajectory of the object's center of mass (top), the pose errors $e_s(t)$ along with the performance functions $\rho_s(t)$ (middle), as well as the velocity error $e_v(t)$ along with the velocity performance functions $\rho_v(t)$ (bottom). It is verified that we achieve tracking of the desired trajectory with prescribed performance. The control inputs (joint torques) as well as the joint velocities are given in Fig. 10. By following the procedure described in the proof of theorem 3, we tune the gains to the values $g_s = 0.05$ and $g_v = 7$ so that the joint torques and velocities respect their respective bounds.

2) *Experimental Results:* We set the desired trajectory in this subsection as in subsection V-A2, i.e., $x_d(t) = 0.3 +$

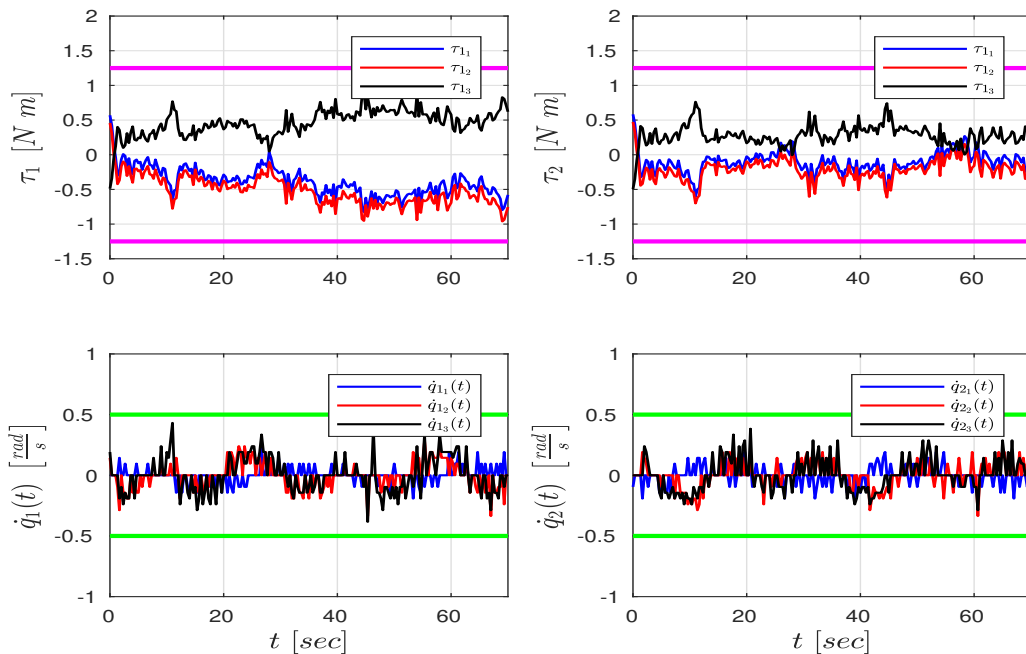


Fig. 7: The agent joint torques and velocities of the experiment of the controller in subsection IV-A, for $t \in [0, 70]$ [sec], with their respective limits (purple and green lines, respectively). Top: The joint torques of agent 1 (left) and agent 2 (right). Bottom: The joint velocities of agent 1 (left) and agent 2 (right).

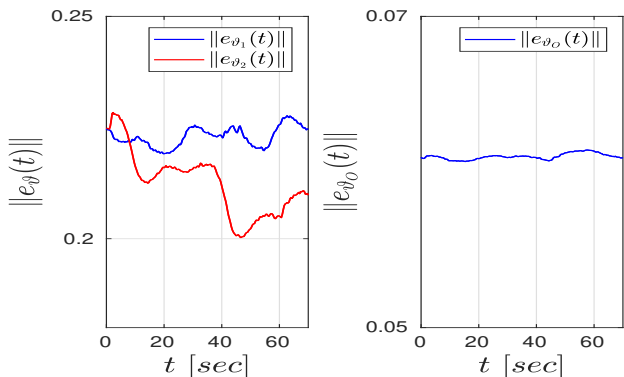


Fig. 8: The norms of the adaptation signals $e_{\vartheta_i}(t), \forall i \in \{1, 2\}$ (left) and $e_{\vartheta_0}(t)$, (right) $\forall t \in [0, 70]$ [sec] of the experiment of the controller in subsection IV-A.

$0.05 \sin\left(\frac{2\pi t}{35}\right)$ [m], $z_d(t) = 0.15 - 0.05 \cos\left(\frac{2\pi t}{35}\right)$ [m], and $\theta_d(t) = \frac{\pi}{20} \sin\left(\frac{5\pi t}{35}\right)$ [rad]. The parameters for the prescribed performance functions are chosen as: $\rho_{s_x}(t) = \rho_{s_z}(t) = 0.03 \exp(-0.2t) + 0.02$ [m], $\rho_{s_\theta}(t) = 0.2 \exp(-0.2t) + 0.2$ [rad], $\rho_{v_x}(t) = 5 \exp(-0.2t) + 5$ [m/s], $\rho_{v_z}(t) = 5 \exp(-0.2t) + 10$ [m/s], and $\rho_{v_\theta}(t) = 4 \exp(-0.2t) + 3$ [m/s]. The values for the gains are set at $g_s = 0.05$ and $g_v = 6.8$. The simulation results are depicted in Figs. 11 and 12; Fig. 11 shows the desired and actual trajectory of the object's center of mass (top), the pose errors $e_s(t)$ along with the performance functions $\rho_s(t)$ (middle), as well as the velocity error $e_v(t)$ along with the velocity performance functions $\rho_v(t)$ (bottom). The prescribed performance tracking can be verified in the experimental case as well. The control inputs (joint torques) as well as the joint velocities are given in Fig. 12, where it is

shown that they respect their corresponding limits.

C. Discussion

It is clear from the aforementioned figures that the tracking of the desired trajectory is achieved by both controllers in the computer simulation and experimental cases. It is worth noting first the difference between the simulations and experiments, which, for both control protocols, lies in the velocity errors. The latter present some oscillatory behavior in the experimental case, which can be attributed to sensor noise, external disturbances/model uncertainties, or inaccuracies/delays of the internal ArbotiX-M controller. The same reason led us to choose slower desired trajectories for the real-time experiments. Nonetheless, these oscillations do not affect the overall tracking performance; Recall that for the Prescribed Performance Controller, tracking of the desired trajectory does not require the functions $\rho_{v_k}(t)$ - and hence the velocity errors e_{v_k} , $k \in \mathcal{K}$ - to asymptotically approach zero.

Among the two control schemes, we can notice a slightly more aggressive behavior of the joint velocities and torques for the Prescribed Performance Controller, which can be attributed to the virtual force that “pushes” the errors e_{s_k}, e_{v_k} not to hit the bounds of the performance functions $\rho_s(t), \rho_v(t)$, respectively, $\forall k \in \mathcal{K}$. Note, however, that this methodology does not require knowledge of the structure of the dynamic terms $M_i(q_i), C_i(q_i, \dot{q}_i), g_i(q_i)$, whose derivation can be tedious, and yields thus significantly lower analytic complexity, without sacrificing the actual performance.

VI. CONCLUSION AND FUTURE WORK

We presented two novel decentralized control protocols for the cooperative manipulation of a single object by N

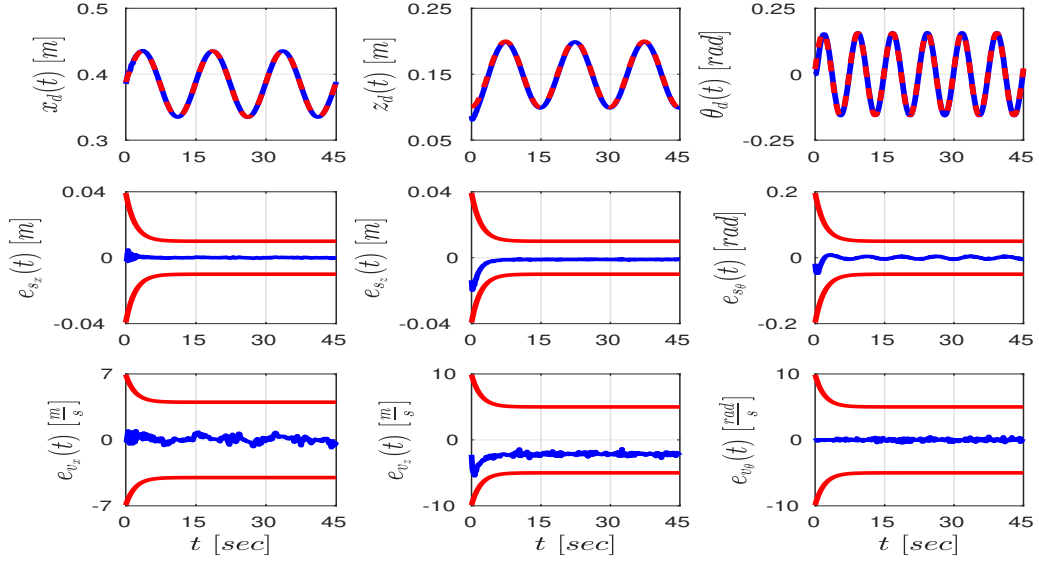


Fig. 9: Simulations results for the controller of subsection IV-B, for $t \in [0, 45]$ [sec]. Top: The desired (with blue) and actual (with red) object trajectory in x -, z -axis, and around y -axis. Middle: The pose errors $e_s(t)$ (with blue), as well as the performance functions $\rho_s(t)$ (with red), respectively. Bottom: The velocity errors $e_v(t)$ (with blue), as well as the performance functions $\rho_v(t)$ (with red), respectively.

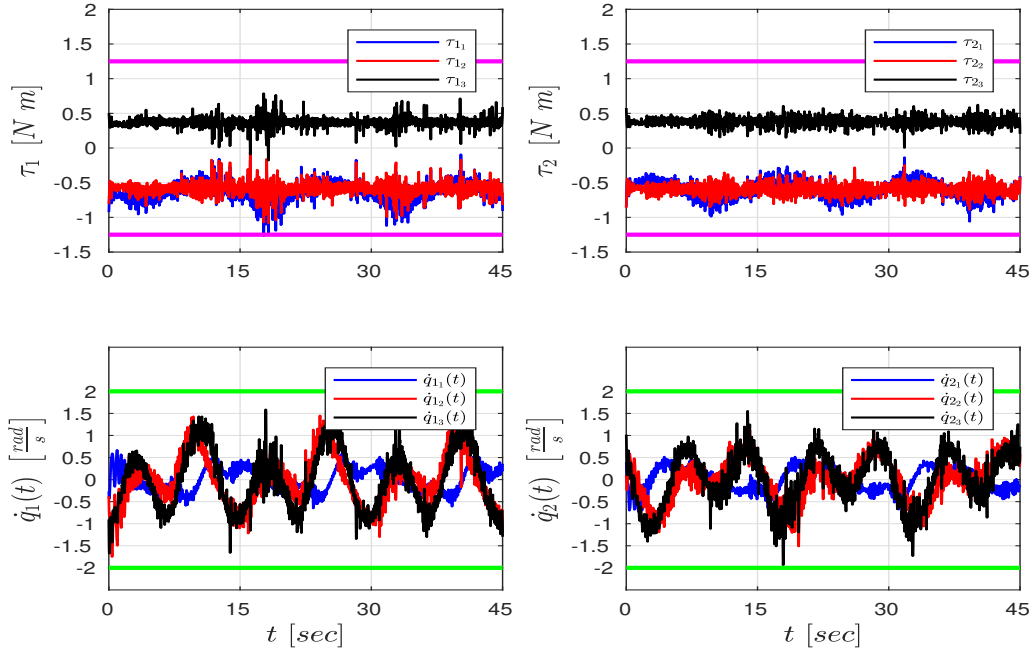


Fig. 10: The agent joint torques and velocities of the simulation of the controller in subsection IV-B, for $t \in [0, 45]$ [sec], with their respective limits (purple and green lines, respectively). Top: The joint torques of agent 1 (left) and agent 2 (right). Bottom: The joint velocities of agent 1 (left) and agent 2 (right).

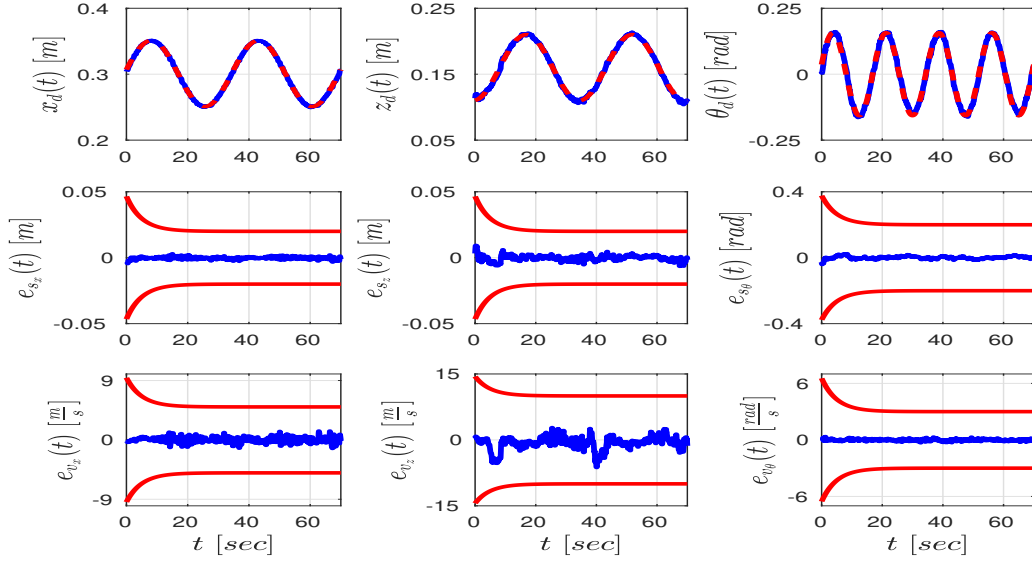


Fig. 11: Experimental results for the controller of subsection IV-B, for $t \in [0, 45]$ [sec]. Top: The desired (with blue) and actual (with red) object trajectory in x -, z -axis, and around y -axis. Middle: The pose errors $e_s(t)$ (with blue), as well as the performance functions $\rho_s(t)$ (with red), respectively. Bottom: The velocity errors $e_v(t)$ (with blue), as well as the performance functions $\rho_v(t)$ (with red), respectively.

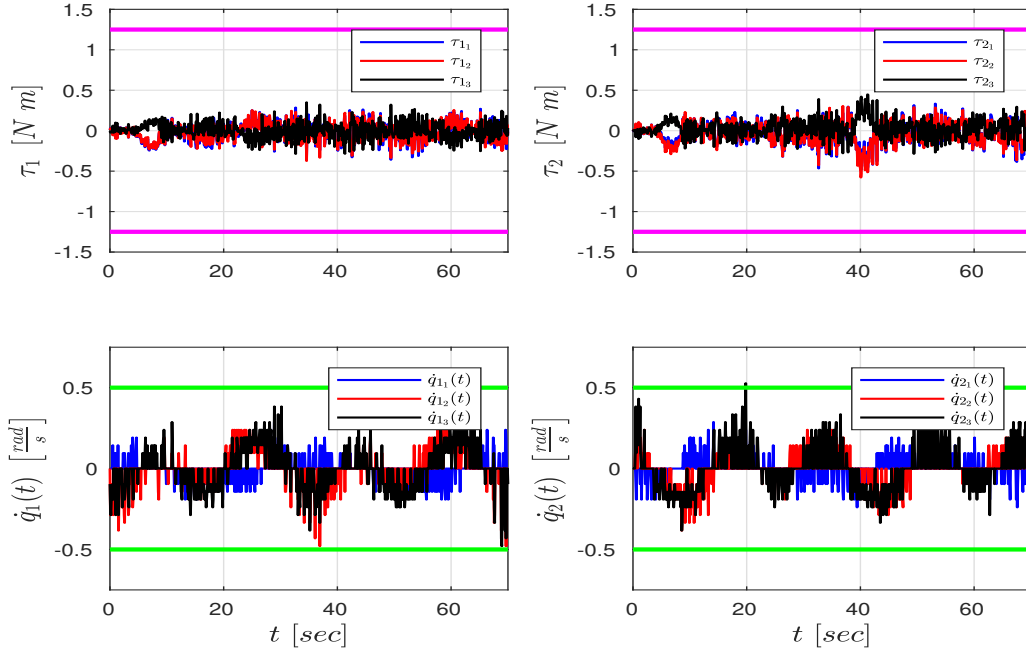


Fig. 12: The agent joint torques and velocities of the experiment of the controller in subsection IV-B, for $t \in [0, 45]$ [sec], with their respective limits (purple and green lines, respectively). Top: The joint torques of agent 1 (left) and agent 2 (right). Bottom: The joint velocities of agent 1 (left) and agent 2 (right).

robotics agents. Firstly, we developed a quaternion-based approach that avoids representation singularities with adaptation laws to compensate for dynamic uncertainties. Secondly, we developed a robust control law that guarantees prescribed performance for the transient and steady state of the object. Both methodologies were validated via realistic simulations and experimental results. Future efforts will be devoted towards applying the proposed techniques to cases with non rigid grasping points as well as uncertain object geometric characteristics.

REFERENCES

- [1] S. A. Schneider and R. H. Cannon, "Object impedance control for cooperative manipulation: Theory and experimental results," *IEEE Transactions on Robotics and Automation*, vol. 8, no. 3, pp. 383–394, 1992.
- [2] T. G. Sugar and V. Kumar, "Control of cooperating mobile manipulators," *IEEE Transactions on robotics and automation*, vol. 18, no. 1, pp. 94–103, 2002.
- [3] O. Khatib, K. Yokoi, K. Chang, D. Ruspini, R. Holmberg, and A. Casal, "Decentralized cooperation between multiple manipulators," *IEEE International Workshop on Robot and Human Communication*, pp. 183–188, 1996.
- [4] Y.-H. Liu, S. Arimoto, and T. Ogasawara, "Decentralized cooperation control: non-communication object handling," *Proceedings of the IEEE Conference on Robotics and Automation (ICRA)*, vol. 3, pp. 2414–2419, 1996.
- [5] Y.-H. Liu and S. Arimoto, "Decentralized adaptive and nonadaptive position/force controllers for redundant manipulators in cooperations," *The International Journal of Robotics Research*, vol. 17, no. 3, pp. 232–247, 1998.
- [6] M. Zribi and S. Ahmad, "Adaptive control for multiple cooperative robot arms," *Proceedings of the IEEE International Conference on Decision and Control (CDC)*, pp. 1392–1398, 1992.
- [7] J. Gudiño-Lau, M. A. Arteaga, L. A. Munoz, and V. Parra-Vega, "On the control of cooperative robots without velocity measurements," *IEEE Transactions on Control Systems Technology*, vol. 12, no. 4, pp. 600–608, 2004.
- [8] J. T. Wen and K. Kreutz-Delgado, "Motion and force control of multiple robotic manipulators," *Automatica*, vol. 28, no. 4, pp. 729–743, 1992.
- [9] T. Yoshikawa and X.-Z. Zheng, "Coordinated dynamic hybrid position/force control for multiple robot manipulators handling one constrained object," *The International Journal of Robotics Research*, vol. 12, no. 3, pp. 219–230, 1993.
- [10] C. D. Kopf, "Dynamic two arm hybrid position/force control," *Robotics and Autonomous Systems*, vol. 5, no. 4, pp. 369–376, 1989.
- [11] F. Caccavale, P. Chiacchio, and S. Chiaverini, "Task-space regulation of cooperative manipulators," *Automatica*, vol. 36, no. 6, pp. 879–887, 2000.
- [12] F. Caccavale, P. Chiacchio, A. Marino, and L. Villani, "Six-dof impedance control of dual-arm cooperative manipulators," *IEEE/ASME Transactions On Mechatronics*, vol. 13, no. 5, pp. 576–586, 2008.
- [13] D. Heck, D. Kostić, A. Denasi, and H. Nijmeijer, "Internal and external force-based impedance control for cooperative manipulation," *Proceedings of the IEEE European Control Conference (ECC)*, pp. 2299–2304, 2013.
- [14] S. Erhart and S. Hirche, "Adaptive force/velocity control for multi-robot cooperative manipulation under uncertain kinematic parameters," *Proceedings of the IEEE/RSJ International Conference on Intelligent Robots and Systems (IROS)*, pp. 307–314, 2013.
- [15] S. Erhart, D. Sieber, and S. Hirche, "An impedance-based control architecture for multi-robot cooperative dual-arm mobile manipulation," *Proceedings of the IEEE/RSJ International Conference on Intelligent Robots and Systems (IROS)*, pp. 315–322, 2013.
- [16] Y. Kume, Y. Hirata, and K. Kosuge, "Coordinated motion control of multiple mobile manipulators handling a single object without using force/torque sensors," *Proceedings of the IEEE/RSJ International Conference on Intelligent Robots and Systems (IROS)*, pp. 4077–4082, 2007.
- [17] J. Szewczyk, F. Plumet, and P. Bidaud, "Planning and controlling cooperating robots through distributed impedance," *Journal of Robotic Systems*, vol. 19, no. 6, pp. 283–297, 2002.
- [18] A. Tsiamis, C. K. Verginis, C. P. Bechlioulis, and K. J. Kyriakopoulos, "Cooperative manipulation exploiting only implicit communication," *Proceedings of the IEEE/RSJ International Conference on Intelligent Robots and Systems (IROS)*, pp. 864–869, 2015.
- [19] F. Ficuciello, A. Romano, L. Villani, and B. Siciliano, "Cartesian impedance control of redundant manipulators for human-robot co-manipulation," *Proceedings of the IEEE/RSJ International Conference on Intelligent Robots and Systems (IROS)*, pp. 2120–2125, 2014.
- [20] A.-N. Ponce-Hinestroza, J.-A. Castro-Castro, H.-I. Guerrero-Reyes, V. Parra-Vega, and E. Olguyn-Dyaz, "Cooperative redundant omnidirectional mobile manipulators: Model-free decentralized integral sliding modes and passive velocity fields," *Proceedings of the IEEE International Conference on Robotics and Automation (ICRA)*, pp. 2375–2380, 2016.
- [21] W. Gueaieb, F. Karray, and S. Al-Sharhan, "A robust hybrid intelligent position/force control scheme for cooperative manipulators," *IEEE/ASME Transactions on Mechatronics*, vol. 12, no. 2, pp. 109–125, 2007.
- [22] Z. Li, C. Yang, C. Y. Su, S. Deng, F. Sun, and W. Zhang, "Decentralized fuzzy control of multiple cooperating robotic manipulators with impedance interaction," *IEEE Transactions on Fuzzy Systems*, vol. 23, no. 4, pp. 1044–1056, 2015.
- [23] K. Tzierakis and F. Koumboulis, "Independent force and position control for cooperating manipulators," *Journal of the Franklin Institute*, vol. 340, no. 6, pp. 435–460, 2003.
- [24] A. Marino, "Distributed adaptive control of networked cooperative mobile manipulators," *IEEE Transactions on Control Systems Technology*, 2017.
- [25] M. Ciocarlie, F. M. Hicks, R. Holmberg, J. Hawke, M. Schlicht, J. Gee, S. Stanford, and R. Bahadur, "The velo gripper: A versatile single-actuator design for enveloping, parallel and fingertip grasps," *The International Journal of Robotics Research*, vol. 33, no. 5, pp. 753–767, 2014.
- [26] F. Aghili, "Adaptive control of manipulators forming closed kinematic chain with inaccurate kinematic model," *IEEE/ASME Transactions on Mechatronics*, vol. 18, no. 5, pp. 1544–1554, 2013.
- [27] J.-H. Jean and L.-C. Fu, "An adaptive control scheme for coordinated multimaniplator systems," *IEEE Transactions on Robotics and Automation*, vol. 9, no. 2, pp. 226–231, 1993.
- [28] D. Sun and J. K. Mills, "Adaptive synchronized control for coordination of multirobot assembly tasks," *IEEE Transactions on Robotics and Automation*, vol. 18, no. 4, pp. 498–510, 2002.
- [29] A. Petitti, A. Franchi, D. Di Paola, and A. Rizzo, "Decentralized motion control for cooperative manipulation with a team of networked mobile manipulators," *Proceedings of the IEEE International Conference on Robotics and Automation (ICRA)*, pp. 441–446, 2016.
- [30] Z. Wang and M. Schwager, "Multi-robot manipulation with no communication using only local measurements," *Proceedings of the IEEE Conference on Decision and Control (CDC)*, pp. 380–385, 2015.
- [31] X. Yun, "Object handling using two arms without grasping," *The International Journal of Robotics Research*, vol. 12, no. 1, pp. 99–106, 1993.
- [32] J. Alonso-Mora, S. Baker, and D. Rus, "Multi-robot formation control and object transport in dynamic environments via constrained optimization," *The International Journal of Robotics Research*, vol. 36, no. 9, pp. 1000–1021, 2017.
- [33] H. Bai and J. T. Wen, "Cooperative load transport: A formation-control perspective," *IEEE Transactions on Robotics*, vol. 26, no. 4, pp. 742–750, 2010.
- [34] H. G. Tanner, S. G. Loizou, and K. J. Kyriakopoulos, "Nonholonomic navigation and control of cooperating mobile manipulators," *IEEE Transactions on Robotics and Automation*, vol. 19, no. 1, pp. 53–64, 2003.
- [35] T. D. Murphey and M. Horowitz, "Adaptive cooperative manipulation with intermittent contact," *Proceedings of the IEEE International Conference on Robotics and Automation (ICRA)*, pp. 1483–1488, 2008.
- [36] A. Nikou, C. K. Verginis, S. Heshmati-alamdari, and D. V. Dimarogonas, "A nonlinear model predictive control scheme for cooperative manipulation with singularity and collision avoidance," *Mediterranean Conference on Control and Automation*, 2017.
- [37] I. D. Walker, R. A. Freeman, and S. I. Marcus, "Analysis of motion and internal loading of objects grasped by multiple cooperating manipulators," *The International journal of robotics research*, vol. 10, no. 4, pp. 396–409, 1991.
- [38] D. Williams and O. Khatib, "The virtual linkage: a model for internal forces in multi-grasp manipulation," *IEEE International Conference on Robotics and Automation*, vol. 1, pp. 1025–1030, 1993.

- [39] J. H. Chung, B.-Y. Y. W. K., and Kim, "Analysis of internal loading at multiple robotic systems," *Journal of mechanical science and technology*, vol. 19, no. 8, pp. 1554–1567, 2005.
- [40] S. Erhart and S. Hirche, "Internal force analysis and load distribution for cooperative multi-robot manipulation," *IEEE Transactions on Robotics*, vol. 31, no. 5, pp. 1238–1243, 2015.
- [41] —, "Model and analysis of the interaction dynamics in cooperative manipulation tasks," *IEEE Transactions on Robotics*, vol. 32, no. 3, pp. 672–683, 2016.
- [42] J.-J. E. Slotine and W. Li, "On the adaptive control of robot manipulators," *The International Journal of Robotics Research*, vol. 6, no. 3, pp. 49–59, 1987.
- [43] B. Siciliano, L. Sciavicco, L. Villani, and G. Oriolo, *Robotics: modelling, planning and control*. Springer Science & Business Media, 2010.
- [44] C. K. Verginis, M. Mastellaro, and D. V. Dimarogonas, "Robust quaternion-based cooperative manipulation without force/torque information," *World Congress of the International Federation of Automatic Control*, 2017.
- [45] C. P. C. P. Bechlioulis and G. A. Rovithakis, "Robust adaptive control of feedback linearizable mimo nonlinear systems with prescribed performance," *IEEE Transactions on Automatic Control*, vol. 53, no. 9, pp. 2090–2099, 2008.
- [46] C. P. Bechlioulis, M. V. Liarokapis, and K. Kyriakopoulos, "Robust model free control of robotic manipulators with prescribed transient and steady state performance," *IEEE/RSJ International Conference on Intelligent Robots and Systems (IROS 2014)*, pp. 41–46, 2014.
- [47] Y. Karayiannidis and Z. Doulgeri, "Model-free robot joint position regulation and tracking with prescribed performance guarantees," *Robotics and Autonomous Systems*, vol. 60, no. 2, pp. 214–226, 2012.
- [48] Z. Doulgeri, Y. Karayiannidis, and O. Zoidi, "Prescribed performance control for robot joint trajectory tracking under parametric and model uncertainties," *Mediterranean Conference on Control and Automation, 2009 (MED)*, pp. 1313–1318, 2009.
- [49] C. K. Verginis and D. V. Dimarogonas, "Timed abstractions for distributed cooperative manipulation," *Autonomous Robots*, pp. 1–19, 2017.
- [50] E. D. Sontag, *Mathematical control theory: deterministic finite dimensional systems*. Springer Science & Business Media, 2013, vol. 6.
- [51] R. Campa, K. Camarillo, and L. Arias, "Kinematic modeling and control of robot manipulators via unit quaternions: Application to a spherical wrist," *Proceedings of the IEEE Conference on Decision and Control (CDC)*, pp. 6474–6479, 2006.
- [52] J.-J. E. Slotine, W. Li *et al.*, *Applied nonlinear control*. prentice-Hall Englewood Cliffs, NJ, 1991, no. 1.
- [53] S. P. Bhat and D. S. Bernstein, "A topological obstruction to continuous global stabilization of rotational motion and the unwinding phenomenon," *Systems & Control Letters*, vol. 39, no. 1, pp. 63–70, 2000.
- [54] C. G. Mayhew, R. G. Sanfelice, and A. R. Teel, "Quaternion-based hybrid control for robust global attitude tracking," *IEEE Transactions on Automatic Control*, vol. 56, no. 11, pp. 2555–2566, 2011.
- [55] T. Lee, M. Leok, and N. H. McClamroch, "Control of complex maneuvers for a quadrotor uav using geometric methods on $se(3)$," *arXiv:1003.2005*, 2010.
- [56] E. Rohmer, S. P. Singh, and M. Freese, "V-rep: a versatile and scalable robot simulation framework," *Proceedings of The International Conference on Intelligent Robots and Systems (IROS)*, 2013.
- [57] Trossenrobotics, "Widowx robot arm kit w/ros." [Online]. Available: www.trossenrobotics.com/widowxrobotarm
- [58] Robotis, "Dynamixel actuators." [Online]. Available: www.robotis.us/dynamixel
- [59] Trossenrobotics, "Arbotix-m robocontroller." [Online]. Available: <http://www.trossenrobotics.com/p/arbotix-robot-controller.aspx>